FINAL REPORT

FIBER OPTICS COMPONENT STUDY

N. S. Kapany
D. F. Capellaro
B. G. Phillips

Prepared for
JET PROPULSION LABORATORY
under Contract No. 950612
(Subcontract under NASA Contract NAS7-100)

Submitted by

OPTICS TECHNOLOGY, INC.
901 California Avenue
Palo Alto, California 94304

January 1966

SUMMARY

20133

Vignetting design data on lens-Focon and lens-field flattener systems were generated. Several experimental Focons and field flattener systems were constructed and their performances were compared with those predicted from the theoretical criteria. In general, satisfactory correlation of the predicted and actual performance was achieved.

The Focon fabrication process which was developed in the course of the contract is described in some detail. The resulting Focons were evaluated in terms of line spread function, MTF, vignetting and T/No. Very little effort was expended in improving the already adequate technique used in fabricating field flatteners. However, the effect of applying an absorbing dye to the outer coating of the individual fibers was investigated. The results indicated an improvement of the wide-angle performance of the field flattener.

Fresnelization techniques were not developed in the course of the contract but experimental data on Fresnel lenses were collated and they confirmed the considerable improvement in wide-angle performance which could be attained by means of Fresnelization.

author

This work was performed for the Jet Propulsion Laboratory, California Institute of Technology, sponsored by the National Aeronautics and Space Administration under Contract NAS7-100.

TABLE OF CONTENTS

LIST OF ILLUSTRATIONS

LIST OF ILLUSTRATIONS (Cont'd)

I. INTRODUCTION

In a previous study, the feasibility of using fiber optics conical condensers (FOCONS) and field flatteners to significantly improve the performance of photographic systems was clearly demonstrated.[1] It was shown that by using fiber optics elements, it is possible to design lens-Focon systems that have higher resolution, lower F/No. and wider field coverage than would otherwise be the case. In addition, the incorporation of such Focons will in many instances facilitate the design of a considerably more stable and compact, high speed optical system for use under adverse conditions.

Although the advantages to be gained by using fiber optics elements were well established in the previous program, it was obvious that further development was required for the fabrication of good quality components, particularly Focons, which could be utilized directly by an optical engineer. The program of work described in this report was undertaken to solve the fabrication problems that are associated with Focons, to improve the functional characteristics of field flatteners, to investigate Fresnelization of fiber optics components to reduce vignetting, and to evaluate the performance of systems in which these components are used.

Efforts in the program were directed toward improving the performance of field flatteners and fabricating Focons that would function in optical systems which operate over field angles greater than 10°, with an output speed of about T/1 at a resolution of 80 to 100 cycles/mm, and which have an output format diameter greater than 17 mm. These objectives were partially achieved. However, although considerable time and effort were expended in the fabrication of fiber optics cones and several good Focons were produced, many problems still remain to be solved before these components can be satisfactorily used in high resolution imaging systems. They nevertheless offer considerable gains in speed where image resolution is not a primary consideration. Furthermore, if the resolution specification were reduced to 40 to 60 cycles/mm, it is highly probable that superior quality Focons could be fabricated with very little further development.

During the course of the program, over thirty fiber optics conical condensers were fabricated, and there were continued improvements in the quality of the Focons. Problems associated with cone fracture that resulted from residual stresses in the units were solved to a major extent. However, some inconsistency still remained in the overall quality of even the later cones. Much of this was due to the necessary use of substandard fibers which were not ideally suited to the severe temperature cycling required in the fabrication of the Focons. However, no other fibers were available. The program was generally directed toward the fabrication of Focons that have an input/output format ratio of between 3 and 4, and the components were tested in optical systems capable of generating an output speed of T/1.

---

1. N. S. Kapany, et al., "Ultra-High Speed Electro-Optical Systems Employing Fiber Optics", Final Report under JPL Contract 950136, November 30, 1962.

When they were used with lenses that operated at F/2.5 and F/3. The field angle covered by these Focons was greater than 20°, without Fresnel or field lenses, and the output resolution, neglecting blemishes, was in excess of 80 cycles/mm. When Fresnel field lenses were incorporated in the system, there was a considerable increase in the acceptable field angle of the Focons.

In contrast, however, high resolution, good optical quality field flatteners up to 3 inches in diameter or more could be fabricated on a mass production basis. There is no reason to doubt that such a field flattener could be produced in diameters of 4 to 5 inches or more, even though the program funding was exhausted before a unit of this size could be fabricated. The field flatteners evaluated were capable of covering a total angular field of more than 45° at a resolution greater than 80 cycles/mm. For an evaluation of the performance of a practical field flattener, the 2 inch focal length F/3.5 Sutton lens which was discussed in the previous contract was again employed. This lens, initially designed by R. C. Baker, has a 2-inch radius Petzval focal surface and is substantially diffraction-limited over a hemispherical field, so that the resolution falls off at large field angles as a result of aperture vignetting. Although Sutton lenses have been used successfully for wide angle aerial photography, using spherical photographic plates, they have not earned more general recognition for this reason. However, the lens is ideally suited for demonstrating the resolution capability and overall optical performance of fiber optics field flatteners and Focons. Its resolution is in excess of 450 cycles/mm and this is still greater than that which could be achieved by random dynamic scanning of a fiber optics field flattener manufactured from 5 micron fibers.

As a result of the considerable expenditure of effort in developing techniques for fabrication fiber optics conical condensers of good quality, insufficient funding precluded the development of techniques required to fabricate a Fresnel lens as an integral part of the input face of fiber optics components. The feasibility of using a replication technique for such Fresnelization has been previously demonstrated, but several additional months of effort would be required before such a technique would be ready for a production program. The improvements that can be achieved with Fresnel lenses matched to the input to a fiber optics system were evaluated on both theoretical and practical bases during the program. It has been demonstrated that the total field angle accepted by a Focon system operating at T/1 can be increased from 20° to 40° using Fresnel lenses. Similarly, a theoretical analysis has shown that it would be possible to increase the total field angle accepted by a Sutton lens-fiber optics field flattener system working at F/3.5, from about 50° to up to 120° at an output resolution of 80 to 120 cycles/mm. If a 3:1 Focon is used with this lens and the field flattener is ground and polished in the input to the Focon a field of some 70 to 80° could be accommodated.

A component and system evaluation program was naturally undertaken and although much of the equipment was available, the system for measuring T/No. and vignetting had to be constructed. The evaluation itself was basically confined to the

measurement of:

1. Flux Density Gain

2. T/No., or the effective stop number (F/No.) computed from the flux density gain, after accounting for the transmission losses of the system.

3. Vignetting, or the loss in image flux density with increasing field angle.

4. Modulation Transfer Function (MTF), or the image contrast as a function of spatial frequency for an object function of unity contrast.

5. Photographic Data

The evaluation program successfully verified most of the theoretical conclusions.

In the early phases of the contract, the Jet Propulsion Laboratory was supplied with several fused plates which were to be sealed to the entrance window of a vidicon. Funding problems were encountered in this venture and the vidicons were not available for evaluation. It was intended that the performance of such a vidicon would be evaluated with and without a conical condenser in contact with the fiber optics window. In a later phase of the program, the conical condensers were to be directly fused into the vidicon and a comparison of the two system configurations undertaken. Since these components were not available, work on this phase of the program was postponed, the funds were exhausted before any such evaluation could be performed.

II. TECHNICAL DISCUSSION

A. Lens-Focon System Design

Typical lens-Focon optical systems are shown schematically in Figure 1a, b and c. In Figure 1a, a conventional flat field lens images the object field in the input face of the conical condenser. As this image passes through the Focon, its size is reduced, resulting in an increase in image flux density. If the ratio of the diameters at the entrance and exit pupils of the Focon is D_1/D_2 (= cone ratio), the gain in flux density will be $(D_1/D_2)^2$, as long as there is no transmission loss through the unit. This means that the photographic speed of the system is increased, and if the F/No. of the input lens is F_i, the equivalent F/No. F_o at the system output will be $(D_2/D_1)\,F_i$, as long as the N.A. of the system output, determined from F_o, is less than the numerical aperture of an individual cylindrical fiber and all the rays from the input lens to the Focon are within the input numerical aperture of the Focon at the point of incidence. It follows, that for a constant F_i, vignetting will ensue with increasing field angle since, firstly, the lower rim ray and, subsequently, the meridional and upper rim ray fall outside the input numerical aperture of the Focon, which is given by (D_2/D_1) (Fiber N.A.). This form of vignetting can be eliminated by incorporating a field or Fresnel lens at the Focon input to bend the meridional ray from the lens along the axis of the individual conical fiber at the point of incidence. A Focon lens system using such a Fresnel field lens is shown schematically in Figure 1b. The Focon is often used with concentric lens systems and the input of the Focon is then ground and polished to fit the spherical Petzval image surface of such a system as shown in Figure 1c.

Figure 2 is a schematic of a lens-Focon system which shows the meridional and lower rim rays. These rays subtend angles of θ_F and θ_{LR} respectively with the optical axis of the lens system.

Several of the parameters associated with the following analysis are shown in Figure 2. Now we have:

$$\text{N.A. of Fiber} = \sqrt{n_1^2 - n_2^2} \tag{1}$$

$$\text{N.A. at Focon Output} = \sqrt{n_1^2 - n_2^2} \tag{2}$$

$$\text{N.A. at Focon Input} = (D_2/D_1)\sqrt{n_1^2 - n_2^2} \tag{3}$$

If the fiber is normal to the input face, and $\theta_{(max)}$ is the maximum angle of incidence which will be transmitted without attenuation along the conical fiber, then:

$$\sin\theta_{(max)} = (D_2/D_1)\sqrt{n_1^2 - n_2^2} \tag{4}$$

If D_1 and D_2 are the input and output diameter respectively and the F/No. of the imaging lens is F_i, then the F/No. of the system at the Focon output if given by

$$F_o = (D_2/D_1) F_i \tag{5}$$

if there is no loss in transmission through the Focon.

Now $\theta_{LR} < \theta_{max}$ given by Eq. 4 and

$$\tan \theta_{LR} = (A_i/2) + f_i \tan \theta_F / f_i$$

where A_i is the diameter of the aperture stop in the lens.

$$\tan \theta_{LR} = (1/2F_i) + \tan \theta_F < \tan \theta_{max}$$

or

$$\tan \theta_F \leq \tan \theta_{max} - (1/2F_i) \tag{6}$$

$$= \tan \theta_{F(max)}$$

If a field lens of focal length $f_L = f_i$ is placed in contact with the cone, then the meridional ray will be bent along the axis so that

$$(1/2F_i) \leq \tan \theta_{max} \tag{7}$$

and

$$(1/2F_o) \leq \tan \alpha$$

where $\sin \alpha$ = fiber N.A. It should be remembered that θ_{max} is a function of the cone ratio D_1/D_2.

A family of curves are plotted in Figure 3, which shows the variation in $\tan \theta_{max}$ as a function of the cone ratio D_1/D_2 with the F/No. of the input lens as parameter. These curves were plotted for the case of fibers that have a N.A. of 0.97 with a core refractive index of 1.79 and a coating glass index of 1.5. The curve at $F_i = \infty$ is a plot of $\tan \theta_{max}$, and if an optimum field lens is utilized $(1/2F_i) < \tan \theta_{max}$.

If a line at $\tan \theta_{max}$ = constant is drawn on the family of curves in Figure 3, this line will intersect the various curves F_i = constant at various cone ratios D_1/D_2, where the ratio is the maximum allowable ratio for no vignetting. From this data we can plot a second series of curves, Figure 4, showing the minimum output F/No. $F_{o(min)}$ (i.e., maximum system speed) which can be achieved as a function of input F/No. with the maximum allowable field angle $\theta_{F(max)}$ as a parameter.

Similarly, if a line D_1/D_2 = constant is drawn on the family of curves in Figure 3, we can plot two sets of curves, Figures 5 and 6, which show the maximum field angle that can be achieved as a function of input and output F/No. respectively, with the cone ratio as a parameter. Since an output format of 17 mm was required in the system, and the cone development program was initially directed toward the production of cones with a maximum diameter of approximately 50 mm, a maximum cone ratio of 3 was feasible. Boundaries that correspond to a maximum cone ratio of 3 and 4 have been incorporated in Figures 3, 4 and 5.

Several lens-Focon systems were designed using these curves to establish a system which could be used for evaluation. For a total field of 10° (without the use of a field or Fresnel lens at the cone input) at an output F/No. of 0.7, it was immediately seen from Figure 4 that a lens with an F/No. of 2 would be required. In subsequent calculations, using the data on field angle, output format and cone ratio, it was established that the lens should have a focal length of 300 mm. Similarly, if a lens having an F/No. of 2.5 were used to cover a total field angle of 16°, an equivalent F/No. at the output of the cone of 0.85 could be achieved. In this system the lens would have a focal length of 180 mm.

If a Fresnel lens or a field lens with a focal length equal to that of the objective lens is used at the cone input, the system design for no vignetting in the cone itself is independent of the field angle when

$$(1/2F_i) \leq \tan\theta_{max} = \tan\theta_{max}\left[\text{function of } (D_1/D_2)\right]$$

i.e.,

$$F_i > F_{i(min)}\left[\text{function of } (D_1/D_2)\right]$$

Figure 7 is a plot of $F_{i(min)}$ as a function of (D_1/D_2) and, obviously, this condition is not a severe design restriction since an output speed equivalent to $F_o = 0.5$ can be readily achieved using any available lens. However, if a field lens is used, the F/No. F_L of the field lens will pose a problem. The focal length of the field lens will be f_i and the aperture will be $D_1 = 2f_i \tan\theta_F$, whence $F_L = (1/2\tan\theta_F)$. The required field lens F/No. F_L is plotted in Figure 8 as a function of semi-field angle θ_F. Considerable aberrations in the image will occur if low F/No. conventional field lenses are utilized. This problem can be readily solved by using Fresnel lenses. Semi-field angle up to approximately 4° could be covered using conventional lenses but in order to cover semi-fields up to 20° or more, Fresnel lenses would be required.

If a cone having an output format of 17 mm and a core ratio of 3 is again utilized, then from Figure 7, the minimum F_o which can be achieved is (1.44/3) = 0.48. If a Fresnel lens with an F/No. of 2.8 can be incorporated, then the semi-field angle which can be tolerated corresponds to 10° and, since the input format = 51 mm, the focal length of the objective lens must be (25.5/tan 10 = 145 mm). Lenses

having an F/No. of 4 at this focal length are not readily available. However, since the image plane resolution of the objective lens need not be much better than 30 to 40 cycles/mm to give an output resolution of 90 to 120 cycles/mm (due to the cone ratio), a lens having an F/No. of 2 or less could be easily found. With such a lens an equivalent output F/No. of 0.66 could be achieved for a semi-field of 10° and the T/No. of such a system would certainly be less than T/1.

B. Field Flattener Design Data

The mechanism of image transfer down the individually coated fibers in fused fiber optics elements has been discussed exhaustively in the literature. Light will be transmitted down the fibers with negligible attenuation if the rays in the fiber core are incident at the core-coating interface at angles greater than the critical angle. This condition will determine the maximum angle α which a meridional ray may make with the fiber axis, for transmission without attenuation due to boundary reflections. The maximum value of α is determined by the N.A. of the individual fibers and is given by $\sin\alpha = \sqrt{n_1^2 - n_2^2}/n_1$, where n_1 and n_2 are the refractive indices of the core and coating respectively. As a result of refraction at the oblique input face of a fiber, the transmitted incident rays must be contained within the angular range θ_1 to θ_2 where θ_1 and θ_2 are again measured with respect to the fiber axis as shown in Figure 9; if β is the oblique angle of the fibers, then:

$$\theta_1 = \arcsin\left[n_1 \sin(\alpha+\beta)\right] \quad -\beta \leq 90 - \beta$$

$$\theta_2 = \arcsin\left[n_1 \sin(\alpha-\beta)\right] \quad +\beta$$

$$|\theta_2| \leq 90 + \beta$$

θ_1 and θ_2 are plotted in Figure 10 for fibers having N.A. of 0.97 and 0.73 respectively. For a conical condenser having a field flattener ground and polished in the input face $\sin\alpha = (D_2/D_1)\left(\sqrt{n_1^2 - n_2^2}/n_1\right)$ and a similar set of curves for θ_1, θ_2 can be plotted as a function of D_1/D_2. These curves are plotted in Figures 11 and 12 for fibers having N.A.'s of 0.97 and 0.73 respectively.

The design of the field flattener used with the Sutton lens is such that the obliquity angle β is identically equal to the corresponding field angle. As a result, the values of θ for the upper and lower rim rays and the meridional ray, θ_{UR}, θ_{LR} and θ_M respectively can all be plotted as a function of β. These plots are superimposed on the curves of Figure 10 and 11. It is immediately obvious that if the rays from the lens could be bent using a Fresnel lens, a semi-field angle of some 60° could be achieved. However, this is not necessarily possible as a result of the requirements on the Fresnel input surface. If γ is the obliquity of the input face of the Fresnel lens at the point of incidence (here γ is measured in the opposite sense to β, the obliquity of the fiber input face) and 2ξ is the vertex angle for the incident cone of light from the objective lens, then the maximum value

of γ is given by

$$\gamma = 90 - \theta_M - \xi$$

where θ_M is the angle of the meridional ray and corresponds to the field angle of the system. Then the angle that the ray refracted at the Fresnel lens input makes with the optical axis is θ', where

$$n' \left[\sin (\gamma - \theta') \right] = \sin (90 - \xi)$$

$$= \cos \xi \doteqdot 0.99$$

$$\sin (\gamma - \theta') = (0.99/n') = (0.99/1.5) = 0.66$$

$$\gamma - \theta' = 41^\circ$$

$$\theta' = \gamma - 41 = 90 - \theta_M - \xi - 41, \text{ where } \xi \doteqdot 8$$

$$\theta' = 41 - \theta_M$$

We wish to compute the angle which this ray makes with the axis at the input to the field flattener itself assuming that there is an air interface between the Fresnel lens and the field flattener. This angle can then be compared with the angles θ_1 and θ_2 of Figures 10, 11 and 12.

$$\sin (\theta'' + \beta) = n' \sin (\theta' + \beta)$$

i.e.,

$$\sin (\theta'' + \theta_M) = n' \sin (41 - \theta_M + \theta_M)$$

$$\sin (\theta'' + \theta_M) = n' \sin 41 = 1.5 \times 0.66 = 99$$

whence

$$\theta'' + \theta_M \doteqdot 90$$

$$\theta'' = 90 - \theta_M \longrightarrow 90 - \beta$$

which is already plotted in Figures 10 and 11 where $\theta_M = 60$; $\theta'' = 30$.

Hence in this instance, with an F/3.5 objective lens and a Fresnel surface fabricated from a material having a refractive index of 1.5, there is no restriction due to the requirements on the Fresnel surface.

It follows from the curves of Figure 10 that if an F/3.5 Sutton lens is used with the field flattener, a total field of approximately 120° could be accommodated by incorporating a Fresnelized surface on the input to the field flattener. Similarly

if a cone ratio of 3 is utilized, a total field of approximately 80° could be accommodated by using optimum Fresnelization.

The above analysis has been carried out on the basis of image vignetting where the rays incident at the fiber input escape from the fibers before they emerge at the output of the field flattener. Much of the light which escapes from the fiber emerges at the output plane of the field flattener after numerous reflections and refractions in the body of the unit. This light contains no image detail but serves to reduce the image contrast. It is apparent then, that any means which can be found to reduce the image vignetting will also increase the image contrast and resolution. Accordingly, if the light which escapes from the fiber core is absorbed, the image contrast and resolution can still be maintained in the presence of vignetting. Furthermore, since some minimal amount of light will always escape from the fiber due to core-coating imperfections, an absorbing coating would improve the contrast and resolution even if no image vignetting takes place. The outer surfaces of the glass coated fibers were coated with an absorbing dye in order to absorb the light which escapes from the fiber core. A fiber optics field flattener containing 3 sections was fabricated using fibers of N.A. = 0.73 and 0.97. One half of the 0.73 fibers were coated with the absorbing dye and the remainder were left uncoated. All of the 0.97 fibers were coated with a less dense absorbing coating. An evaluation of this field flattener was performed and it was established that the absorbing coating improved the contrast and resolution. The data will be presented later in the report.

C. Fiber Optics Condenser Fabrication

The procedure used in the manufacture of fiber optics conical condensers prior to this program was similar to that used in the manufacture of multiple fibers. A 1 to 2 inch diameter boule consisting of an aligned array of individual multiple fibers packed in a glass tube was placed in a vertical furnace and slowly heated to just below the softening temperature of the fibers. The boule was then slowly lowered past an annular heating zone where the glass softened and could be drawn. The drawing was continued until the required cone shape was achieved, at which time the temperature of the heating elements was reduced, and the drawing was continued to maintain the cone shape until the glass viscosity was too high for continued drawing. The boule assembly was then placed in an oven and annealed.

It was obvious at the beginning of the contract that this technique lacked many desirable features and was unlikely to yield high quality Focons. Problems were encountered due to poor tacking and packing of the individual fiber multiples. Gaps between the fiber optics multiples were numerous and the incidence of opaque fibers in the multiples themselves was prolific due to the high temperature cycling required to start the draw.

These experiments did, however, indicate many of the problems which would have to be solved in order to fabricate high quality Focons. For example:

1. Dirt, grease, etc. on the fibers.

2. Entrapped air in the boule assembly.

3. Adsorbed air in the individual fibers of the fiber multiples.

4. Entrapped air in the fiber multiples.

5. Devitrification of the core and/or coating as a result of the number of heat cycles required which encompassed the devitrification temperature range but not the glass-forming range.

6. Thermal strain and annealing from using glasses of different coefficients of expansion and softening temperatures, etc.

7. Distortion in the final component due to non-linear coning of the individual fibers across the Focon diameter: this problem was not significant in the longer cones but some problem was encountered when efforts were made to produce very short cones.

8. Obliquity of the fibers at the input and output. This was not a significant problem but it dictated the shape of the cones since input and output faces which are cut at an oblique angle with respect to the individual fiber are generally less efficient than faces cut normal to the fiber axis.

The development of the necessary techniques for fabricating good cones commenced with a more thorough cleaning process and a more careful packing of the fiber multiples into the 1 to 2 inch diameter glass tubes prior to drawing. The feasibility of packing the boules immediately after drawing the fiber multiples was considered but these fibers acquired a high static charge on their passage through the furnace and, as a result, picked up minute particles of dust, etc., very readily. As such they still had to be cleaned. Nevertheless, every consideration was given to cleaning, assembling and drawing the fibers and boules within as short a time as possible since it had been previously established that the outer surfaces of the fiber multiples (or singles) deteriorated with age and this deterioration was much more significant in the final cone fabrication. Problems were also encountered in the packing of the hexagonal fiber multiples into the circular cross section tubes. Since this problem persisted, circular fiber optics multiples were subsequently drawn and packed into the tubes. However, this made it more difficult to maintain the fiber alignment during the cone fabrication and in the early stages of the work on this process, there was some tendency for the individual fiber multiples to twist with respect to each other during the fabrication cycle so that the image at the Focon output was distorted. This difficulty was solved by placing flats on the side of the circular multiples giving a reference surface by which to locate the fiber position

during drawing.

For greater control over the coning process, the fiber multiple boules were no longer mounted vertically in the drawing machines. Instead, the fibers were assembled in a tube which was very much longer than the individual fibers and the whole assembly was mounted in a glass turner's lathe as shown in Figure 13. The tube assembly was rotated steadily and a cylindrical oven surrounding the boule unit was used to heat the assembly slowly. When the temperature of the boule was just below that of the fiber softening point, a narrow annular heating coil was used to generate the necessary local heating of the central portion of the boule. At the same time, the headstock on the lathe was drawn out slowly and the boule was pulled into a double cone as shown in Figure 14. As soon as the boule started to pull apart, the temperature of the annular heating coil was reduced with the result that as the boule was pulled apart it cooled and the glass viscosity increased. When the boule was too stiff to pull any further, the assembly was removed and placed in an annealing oven.

Some success was achieved in the early stages of this technique, although, in many instances, the optical quality of the fibers deteriorated during fabrication and the resulting conical condensers were of poor transmission and unsatisfactory resolution. Some of the early cones fractured during the annealing cycle but subsequent assemblies used a cylindrical tube having thinner walls and an extended annealing cycle reduced the incidence of cone fracture considerably.

It was thought that much of the fiber deterioration was due to the entrapment and subsequent expansion of air in the multiple fibers. On expanding, this air distorted the core-coating boundary of the fibers so that light escaped from the fibers at this point resulting in a loss in transmission down the distorted fiber and a loss of contrast in the final image. The entrapped gas could arise from two sources. In the first case, gasses which were adsorbed in the surfaces of the fibers were freed during the heat cycle. In the second case, the gasses filled the pockets that were left when the multiples were packed. The gas entrapment took place as the glass softened and tacked itself, so that air which was trapped within the boule was not then able to escape and expanded as the temperature was further increased. On stretching the boule this expanded gas distorted the fiber core-coating boundary. This effect was indicated when a poorly transmitting cone was sliced along a meridional plane containing the axis of symmetry of the cone: fine channels were observed to run for lengths of 1/16 inch or more along the fibers. These channels had obviously distorted the adjacent fibers and the thickness of the coating glass was reduced below the minimum thickness required for total internal reflection to take place at that core-coating boundary.

This problem was avoided by packing the boule assembly into a thin-walled glass tube which was sealed at one end. The assembly was mounted in the lathe as before but, in this case, the open end of the glass tube was connected to a vacuum pump. The unit was heated and before the softening point was reached, the annular heating ring was switched on. In this instance, however, the ring was slowly passed

along the tube from the sealed end to the open end and successive zones of the boule were softened and tacked. After the entire boule length was passed, the vacuum was turned off and the annular heating zone was returned to the boule center. As the center softened, the boule was pulled apart as before to form the cone, and the temperature of the heating ring was reduced so that the viscosity of the glass fibers in the boule increased and further stretching of the boule was prevented. The assembly was then removed from the lathe and placed in an annealing oven before the cutting, grinding and polishing operation.

The incidence of dead fibers along the boundaries of the fiber multiples was reduced considerably by this procedure but there was still an unacceptable number of poorly transmitting fibers within the multiples themselves. This was due to the large number of heat cycles required in which there was an increasing degradation in the individual fiber coatings. A similar but less severe problem had been encountered in the fabrication of fused fiber optics plates and field flatteners. In this instance the problem was completely solved by reducing the final processing temperature and considerably increasing the pressure required to fuse the fiber multiples.

With this situation in mind successive boules were mounted in the lathe, evacuated, and heat cycled as before but the fabrication temperatures of the successive boules were progressively reduced. A considerable improvement in the Focons was achieved, and although the final optical quality was not perfect, it was acceptable for many purposes. Transmissions within 10 percent of the theoretical maximum were achieved and resolutions in excess of 80 cycles/mm seemed feasible.

It is certain that the overall optical quality could be improved by using the techniques described above if larger diameter individual fibers were utilized. The Focon fabrication was undertaken using fibers of 12 to 15 micron diameter so that the fiber size at the output of a 3:1 Focon was less than 5 microns. The fiber coating thickness at the output of such Focons is approximately 1 micron. If fibers with an initial diameter of 25 to 35 microns were utilized, the problems would be considerably alleviated and resolutions in excess of 40 to 50 cycles/mm would still be feasible.

D. Component Evaluation

1. Field Flatteners

The field flattener which was tested was fabricated in three sections. Two of these sections utilized fibers having a numerical aperture of 0.73 and the fibers in one of these sections were coated with an absorbing dye, frequently called "extramural absorption (EMA) coating". The third section of the field flattener had fibers of 0.97 N.A. and these were all EMA-coated but the optical density of the dye was less than that used for the previous section. The input surface of the field flattener was ground and polished to fit the spherical Petzval surface of the F/3.5, 2-inch focal length concentric Sutton lens referred to in the introduction. Data on image vignetting and Modulation Transfer Function (MTF) of the Sutton lens-field flattener camera were obtained for all three segments of the field flattener. Photographs of

the line spread function were obtained at different field angles, and landscape photographs were taken through the completed camera.

a. Vignetting and Transmission

The system vignetting was measured using the equipment shown schematically in Figure 15. An aperture which could be varied from about 1/8 inch diameter to about 2-1/4 inch diameter was illuminated by means of an aspheric condenser lens and a 500w projection lamp. A 24 inch, F/6 Aero Tessar camera lens was used to collimate the light from this aperture. The Sutton lens and field flattener were mounted on a rotating platform and the collimator aperture was set so that the image formed by the Sutton lens was approximately 1/10 inch diameter. The flux that emerged from the field flattener output face was then measured by means of an integrating sphere having an 0.020 inch diameter input aperture and a cadmium sulfide photoconductive cell. Before the vignetting experiments were made, a linearity check was performed on the integrating sphere and cadmium sulfide monitoring system. The calibration curves are plotted in Figure 16 for the two sensitivity ranges utilized in the vignetting and flux density gain measurements.

Figure 17 is a plot of the vignetting of the field flattener and Sutton lens system and these results have been corrected for the cell non-linearity. The vignetting of the Sutton lens itself is also plotted in this figure and follows the theoretical $\cos\theta$ law quite closely. As can be seen from these curves the system vignetting follows the predicted form quite closely for both the high and low numerical aperture field flatteners fabricated from EMA coated fibers where the cut-off occurs at semi-field angles of 36 and 28° respectively. The theoretical cut-offs as determined from Figure 10 would occur at smaller field angles than those predicted by the simple meridional ray theory utilized in the analysis, but a significant fraction of this apparent discrepancy is due to the increasing Fresnel reflection losses at the output of the individual fibers and to losses due to the increasing number of reflections within the fiber core with increasing field angle. The apparent anomaly, which is evident in the case of the field flattener fabricated from uncoated fibers having a numerical aperture of 0.73, occurs because the light which escapes from the fiber core is not absorbed by an EMA coating and reaches the output face of the field flattener. However, this light degrades the output image by reducing its contrast.

In order to measure the flux density gain (= flux per unit area "out"/flux per unit area "in") the field flattener was removed and the integrating sphere, cell and 0.020 inch stop was moved to the primary image position. The on-axis flux density gains of the three field flatteners were 0.59, 0.61 and 0.67 respectively for field flatteners fabricated from EMA-coated 0.97 N.A. fibers, EMA-coated 0.73 N.A. fibers and uncoated 0.73 N.A. fibers. The area occupied by the fiber cores in fused fiber optics elements is approximately 85 percent of the total area. The Fresnel reflection coefficients for normal incidence are approximately 0.08 and 0.067 for cores having a refractive index of 1.79 and 1.67 respectively. Hence the high and low numerical aperture fused fiber optics elements would be expected to

have transmissions of 72 and 74.7 percent respectively when all the transmitted light travels within the fiber core. However, it has been established that the EMA coating fractionally reduces the core transmission since the waves propagated along the fiber core penetrate the core-coating boundary to some extent and energy is absorbed by the dye in the coating glass. (One of the problems encountered in using the absorbing coating was that of preventing the dye from penetrating too close to the core-coating interface.) Since the field flatteners were at least 1/4 inch thick (in their thinnest part), the on-axis transmissions measured in terms of flux density gains were to be expected.

b. Resolution

It has already been indicated that a field flattener fabricated from EMA-coated fibers would maintain the contrast in the image over a wider field angle than one fabricated from uncoated fibers. This is shown in Figure 18 which is a photograph of a series of resolution charts taken through the Sutton lens and three-section field flattener. The photograph shown in the figure was constructed from three negatives obtained by photographing a single horizontal line of 4 resolution charts at different orientations of the camera about the horizontal axis. The resolution charts in the photograph are positioned with respect to the output of the field flattener itself. The right hand section of the field flattener was fabricated from the 0.97 N.A. fibers; the left hand, lower section, was fabricated from uncoated 0.73 N.A. fibers; and the left hand, upper section, was fabricated from EMA-coated 0.73 N.A. fibers. It is evident, however, from this photograph that the top line of the resolution charts were not as accurately focused as the others. This was probably a result of the camera back-tipping so that the film was only in partial contact with the field flattener. However, the increase in contrast due to the EMA is still noticeable. These and other photographic negatives were used to plot the maximum line pair resolution which could be observed in the negatives as a function of the coresponding semi-field angle. These curves are plotted in Figures 19, 20 and 21 for the three sections of the field flattener. The resolution of the system will be higher than the figures indicate, since some loss is resolution certainly at the higher spatial frequencies resulted from the film (Panatomic X). For comparison, the maximum spatial frequency that corresponds to a system maximum MTF of 0.5 has been superimposed on these curves for the various semi-field angles. These curves were obtained from plots of the maximum MTFs of the system which will be discussed later in the report.

The effect of the EMA coating and fiber N.A. can also be observed in the photographs of a bar chart shown in Figures 22 and 23. These photographs were taken through two of the sections of the field flattener. The individual fibers which are easily visible in the photographs are approximately 5 to 7 microns in diameter and the 2-1/2 cycle high frequency bar patterns correspond to a spatial frequency of approximately 47 cycles/mm in the focal plane of the Sutton lens. Figure 22 is a photograph taken through the 0.73 N.A. uncoated field flattener. Figure 23 is a photograph taken through the 0.97 N.A., EMA-coated field flattener and, in this instance, the improvement in contrast and resolution at large field angles is

particularly noticeable. The bar pattern is adequately resolved for both sections of the field flattener for semi-field angles up to at least 15° and this agrees with the MTF measurements which were subsequently obtained.

Fundamentally, it would be preferable to measure the dynamic MTF of the field flattener obtained by randomly scanning the field flattener over an amplitude that corresponds to several fiber diameters. However, in the technique adopted for the MTF measurements, a high numerical aperture oil immersion microscope objective was required to image the line spread function that emerged from the field flattener onto a rotating sinusoidal density masks. As such, it was inconvenient to incorporate dynamic scanning. Furthermore, since the static MTF is a function of fiber pattern orientation, the maximum value of the static MTF was determined to facilitate a ready comparison of the performance of the field flattener at various field angles. A schematic of the apparatus used for measuring the MTF is shown in Figure 24. The maximum MTF was obtained by aligning and centering the diffraction-limited image of an infinitely distant slit formed by the F/3.5 Sutton lens, within a single line of fibers in the input face. The image of the resulting line spread function at the field flattener output face was then carefully focused and aligned with the scanning variable density sinusoidal bar pattern: the flux that passed through the pattern was recorded on a strip chart recorder for subsequent analysis. The minimum value of the static MTF could then be obtained approximately by halving the spatial frequency; it should be noted, however, that with random dynamic scanning of the field flatteners, the MTF at the high spatial frequencies would be greater than the maximum static values measured as indicated above.

Figure 25 shows photographs of the line spread functions which were utilized in measuring the MTFs of the 0.97 N.A. and the 0.73 N.A. segments of the field flattener; the broadening of the line spread function with increasing field angle is particularly evident for the lower N.A. segments. The maximum MTFs of the Sutton lens and the three sections of the field flattener are plotted in Figures 26, 27 and 28 for various semi-field angles. The MTF of the Sutton lens itself was obtained using the same apparatus and is plotted in Figure 29. In a system using non-linear fiber optics elements (which do not really have a MTF in accordance with the generally accepted terminology) the MTF of the system is not the product of the MTFs of the constituent members of the system. However, a comparative measure of the performance of the field flattener can be obtained on the assumption that the MTF exists and can be obtained by dividing the MTF of the Sutton lens into that of the system. These curves are plotted in Figures 30, 31 and 32 for the three sections of the field flattener. These curves indicate, firstly, that the 0.97 N.A. section of the field flattener maintains the image contrast for higher spatial frequency and for wider field angles than the 0.73 N.A. field flattener and that, secondly, the EMA-coated 0.73 N.A. section of the field flattener maintains the image contrast over a wider range of spatial frequency and field angle than the section fabricated from uncoated fibers. Figure 33 is a landscape photograph taken with the Sutton lens and three-section field flattener. Some ghosting of the bright parts of the field were due to multiple reflection in a neutral density filter which had to be used because the camera was operated with a low speed shutter.

The picture does, however, indicate the performance which can easily be achieved using such field flatteners.

2. Focon Performance Data

Typical Focon systems have been previously shown in Figures 1a, b and c. In Figure 1a a conventional flat-field camera lens forms an image on the input to a fiber optics conical condenser. The Fresnel lens shown in Figure 1b is used to reduce the vignetting at large field angles. In Figure 1c, the symmetrical Sutton lens forms a diffraction-limited image on the spherical surface of a fiber optics field flattener, which is followed by a conical condenser to increase the photographic speed of the system. In most instances, as in the example shown, the field flattener and conical condenser will be an integrated fiber optics element. When the conical condenser is used in conjunction with a separate field flattener, the overall transmission and resolution of the system will be less than if an integrated component were utilized. However, since the resolution of a separate field flattener can be significantly greater than that at the input to the conical condenser, the loss in resolution will not be a serious problem. The fibers at the output from the conical condenser cannot be much less than 5 microns for maintaining the transmission and the contrast in the output image. It follows that if a cone ratio of 3 or more is utilized the fiber size at the input to the conical condenser will be greater than 15 microns. However, the fiber size in the field flattener can still be approximately 5 microns so that its resolution is very much greater than that at the input to the conical condenser. Nevertheless, the performance of a system using a separate field flattener and conical condenser was not measured in the course of the contract. Vignetting, T/No., MTF and photographic data were obtained on Focons that had spherical and plane input faces.

a. Cone Vignetting

The vignetting of a large number of Focons was measured during the course of the contract and it was established that the form of the vignetting could be categorized in terms of the Focon type. In the early part of the contract, cones were produced in which the fibers at the input were not parallel to the axis of symmetry of the cone, as shown schematically in Figure 24a. This type of Focon resulted in quite severe vignetting which could be reduced by employing an optimum Fresnel lens. One such unit will be discussed below. The second type of cone is shown in Figure 34b and the vignetting problem in this instance was less severe than in the preceding case and was still further improved by utilizing a suitable Fresnel lens. Most of the cones produced throughout the contract were of this type and the evaluations on some typical examples will be presented below. The last type of Focon is shown in Figure 34c. In this case, a spherical field flattening surface was ground and polished in the focon input and severe vignetting occured because of the resulting obliquity of the fiber input face with respect to the fiber axis. This problem has been previously analyzed in this report and the results on such a Focon will be presented below.

(1) Focon (Type 1)

The vignetting on a Focon in the form shown in Figure 34a is plotted in Figure 35 and the important data pertinent to the particular cone is shown in the inset of Figure 35. As a result of the diameter of the cone input and the focal length of the objective lens, the maximum semi-field angle which could be accommodated was approximately 12°. The fibers at the edge of the field in this particular Focon were inclined at an angle approximately 12° with respect to the optical axis of the system. If we assume a linear relationship between the field angle and the obliquity angle, then $d\beta/d\theta_F = -1$, using same convention as that used for the field flattener analysis. Again β is the angle of obliquity and θ_F is the field angle so that $\theta_F = -\beta$. If an F/4 input beam is utilized, total vignetting will occur for $-2\beta + 7 \geq \theta_2$. Note that θ_2 is negative in the convention of the previous analysis.

If the straight line $\theta(\beta) = -2\beta + 7$ is plotted on the curve of Figure 11, the maximum value of β (and hence the maximum field angle) can be determined from the point of intersection of the straight line with the curve of θ_2 for a cone having a ratio of 3:1. For the cone under investigation, the maximum field angle for complete vignetting is 9° and agrees with the experimental results of Figure 35.

Further computations indicated that a Fresnel lens having a focal length of approximately 20 to 30 mms would eliminate vignetting caused by both the obliquity factor and the field angle. The vignetting curves obtained using Fresnel lenses of 20 and 30 mm focal length are superimposed on the original vignetting curves of Figure 35 and the improvement can be readily seen.

(2) Focon (Type 2)

The vignetting on several Focon systems utilizing Focons of the type shown schematically in Figure 34b are shown in Figures 36, 37, 38 and 39. In these Focons, the obliquity angle $\beta = 0$ and the maximum and minimum angle θ_1 and θ_2 which can be accepted by the Focon are equal in magnitude. If the cone has a ratio of 2.7, the curves in Figures 3 and 11 indicate that $\theta_2 \simeq 19°$ so that if an F/2.5 lens is used, vignetting would be expected to commence at a field angle of 8° and be completed at a field angle of 30°. The vignetting in Figure 36, however, is somewhat more severe than these calculations would indicate, but much of this is due to the poor quality of the fibers and to the high Fresnel reflection losses at the Focon output. The poor quality of the fibers reduces the effective N.A. of the fiber so that vignetting is more pronounced.

(3) Focon (Type 3)

The vignetting curve for a Focon with a field flattener ground and polished in its input face is shown in Figure 40. This Focon was otherwise very similar to that used in plotting the curves of Figure 36. In this instance, however, the vignetting is significantly more severe because of the curved input face. Figure 11 indicates that complete vignetting should be anticipated at a semi-field angle of approximately

15° and agrees quite closely with the experimentally determined, extrapolated cut-off. However, no Focon vignetting should have occurred for semi-field angles less than approximately 7° but, as in the previous case, vignetting occurs for a smaller field than the theoretical analysis predicts. Again, this was almost certainly due to a combination of an effective reduction in the numerical aperture of the fibers as a result of their poor optical quality, together with severe Fresnel reflection losses at the Focon output.

b. Transmission Losses within the Focon

Many of the vignetting measurements indicated a more severe attenuation of the transmitted flux than that which was anticipated from the theoretical analysis. This was thought to be partially due to the increasing Fresnel losses at the conical condenser output as a result of increasing field angle. As can be seen from Figure 41a, rays which are incident on the input face of a cylindrical fiber at large angles of incidence, undergo successive reflection at the fiber core-coating boundary at angles of incidence which are closer to the critical angle at the interface than those which occur for paraxially incident rays. As a result, minor imperfections in the core-coating interface have a much more severe effect on these rays. This problem is considerably accentuated because such rays undergo many more reflections than the paraxial rays. As a result, the effective input numerical aperture of the system is significantly reduced. Furthermore, these wide angle rays are incident at the output face of the cylindrical fiber at larger angles of incidence so that the Fresnel internal reflection losses are more severe.

The Fresnel losses were investigated using the arrangement shown schematically in Figure 41b in which an F/11 beam was used to form an uniformly illuminated image at the center of a good quality Focon. This beam was then scanned over a range of incident angle ψ and the flux that emerged at the output was measured using a calibrated silicon cell. The resulting vignetting curve is plotted in Figure 42. The cell was then optically coupled to the output face of the Focon, using an immersion fluid having a refractive index of 1.62, and a second vignetting curve was then obtained. As can be seen, the vignetting was significantly reduced for angles of incidence greater than about 12°.

The ratio of the input to output diameters of the core used for these experiments was approximately 2.3 and one would expect complete vignetting at angles in excess of approximately 30°. However, the core was not manufactured from EMA-coated fibers and light was able to pass from the coating to the core and from the cores to adjacent cores via the coating glasses. In effect this increased the apparent image transmission, but resulted in a considerable reduction in image contrast. This phenomena, however, did not invalidate the conclusion that the immersion of the cell in the output face reduced the vignetting due to Fresnel reflection losses at the output.

The reduction in the N.A. of the fibers as a result of the surface finish between the core and coating glass was verified using the radiation pattern measuring equipment

drawn schematically in Figure 43. Single and multiple fibers were fabricated in the usual way from solid glass cores which were initially given two types of surface finish. In the first type the solid 1 inch diameter IR 442 cylinders were optically polished in a lathe and in the second type the cylinders were fine-ground using W2 grit. The respective glass rods were placed in fire-polished tubes of R6 and subsequently single and multiple fibers were fabricated in the usual way. Four-foot lengths of the respective fibers were selected and their ends were ground and polished. The radiation patterns of the two types of fibers were measured by fully illuminating the fiber input apertures with a lambertian source and the radiation pattern at the output was scanned with a photomultiplier having a very small entrance pupil. The cross sections of the radiation patterns obtained in this way are plotted in Figure 44 and, as can be seen, the effective numerical aperture is very much less for fibers fabricated from core rods which were fine-ground with W2 compound. One would anticipate that as the interface between the core and coating glass deteriorated, the effective N.A. would be further reduced so that with a very poor interface this reduction in N.A. would occur for much shorter fibers.

c. T/No. and Transmission

The T/Nos. of the overall systems were obtained by experimentally determining the flux density gain of the Focon itself and using this value to compute the T/No. of the overall system, on the assumption that the T/Nos. and F/Nos. of the objective lenses were identical. For the measurement of the flux density gains of the Focons, the equipment used in determining the system vignetting characteristics was again utilized. A large image of the uniformly illuminated collimator aperture was imaged into the focal plane of the system objective lens and the flux that passed through a small aperture stop in this plane, V_1, was measured. The conical condenser was then inserted in the system with its input face coincident with the image (focal) plane of the objective lens. The flux that passed through the same aperture stop placed in contact with the image at the output face of the Focon, V_2, was measured. Then the flux density gain of the Focon was given by V_2/V_1 and varied from 3 to 7-1/2 for Focons with ratios of 2:5 to 4:1. The theoretical flux density gain was calculated from the cone ratio D_1/D_2 and equals $(D_1/D_2)^2$ so that the transmission of the Focon could be calculated. The measured flux density gains and the calculated transmission are tabulated in Table 1 for several of the Focons which were produced during the contract.

For a direct measurement of the transmission of the Focons, the collimator aperture was stopped down and a very small image was focused onto the input face of the Focon. The total flux incident on the Focon, V_3, and the total flux that emerged at the Focon output, V_4, were measured with the integrating sphere and cadmium sulfide cell. The Focon transmission was then given by V_4/V_3. This data is also tabulated in Table 1 and confirms the values calculated from the flux density gain measurements.

d. Resolution

The modulation transfer function of a Focon having a 2 inch radius spherical input face was measured with the same equipment as that used in the measurements on the field flattener. Again the maximum value of the modulation transfer function was obtained for various field angles. The MTF curves for the Sutton lens-Focon system are plotted in Figure 45 and the MTF of the Focon itself is plotted in Figure 46 on the assumption that the MTF of the Focon can be obtained from MTF of system/MTF of Sutton lens. Total fields in excess of 23° could be obtained at minimum resolution in excess of 50 to 60 cycles/mm with such a system. By suitable Fresnelization of the input to the Focon, and using EMA coated fibers in the fabrication process, this performance could be maintained over a larger angular field.

III. CONCLUSIONS

Over thirty Focons were produced during the course of this contract and the optical quality of these Focons has shown a continual improvement. It is now feasible to fabricate Focons having an input format of 40 to 50 mm diameter and having an output resolution in excess of 40 cycles/mm. Photographic speeds in excess of T/1 have been achieved on several occasions, but there is still scope for some improvement in the optical quality of these components. However, the components that are currently available are satisfactory for many purposes.

Fiber optics field flatteners of superior optical performance are available on a production basis in format sizes up to 3 inches in diameter. Larger sizes can be readily produced by joining several smaller units. These components have been used to cover semi-field angles in excess of 25° at resolutions in excess of 80 to 100 cycles/mm. With some development effort in perfecting Fresnelization of the field flattener input, the field angle coverage could be extended to approximately 60° (total field = 120°). The performance of the Sutton lens camera and field flattener which was evaluated during the course of this contract is superior to the performance of many conventional cameras, and the ultimate potential of this system has not yet been attained.

The improvements which could be achieved by means of Fresnelization have been adequately demonstrated in this report. It is imperative that the necessary Fresnelization techniques be developed as soon as possible so that the ultimate potential of both Focons and field flatteners can be attained. Funding on this aspect of a future fiber optics development program will certainly enhance the performance of all current fiber optics components.

With further development effort, there is no reason to suppose that the resolutions and optical quality of current field flatteners and fused plates could not also be achieved with Focons.

TABLE I

Cones	No.	Ratio	Flux Density Gain, X	Transmission Calculated, %	Transmission Measured, %
Early Multiple	-	2.92	3.1	36.5	-
Early Multiple	-	3.1	4.75	49.5	-
Single Fiber	-	3.1	5.9	61.5	60
Multiple Fiber	13a	2.47	3.0	50	-
Multiple Fiber	14a	-	3.2	-	-
Multiple Fiber	14b	2.47	3.2	52	52
Multiple Fiber	18/1	2.7	3.3	45	45.5
Multiple Fiber	18/2	2.66	3.1	43.5	41
Multiple Fiber	24/1	2.3	-	-	50.5
Multiple Fiber	25/1	2.9	4.17	48	46.6
Multiple Fiber	25/2	4.0	7.15	44	45

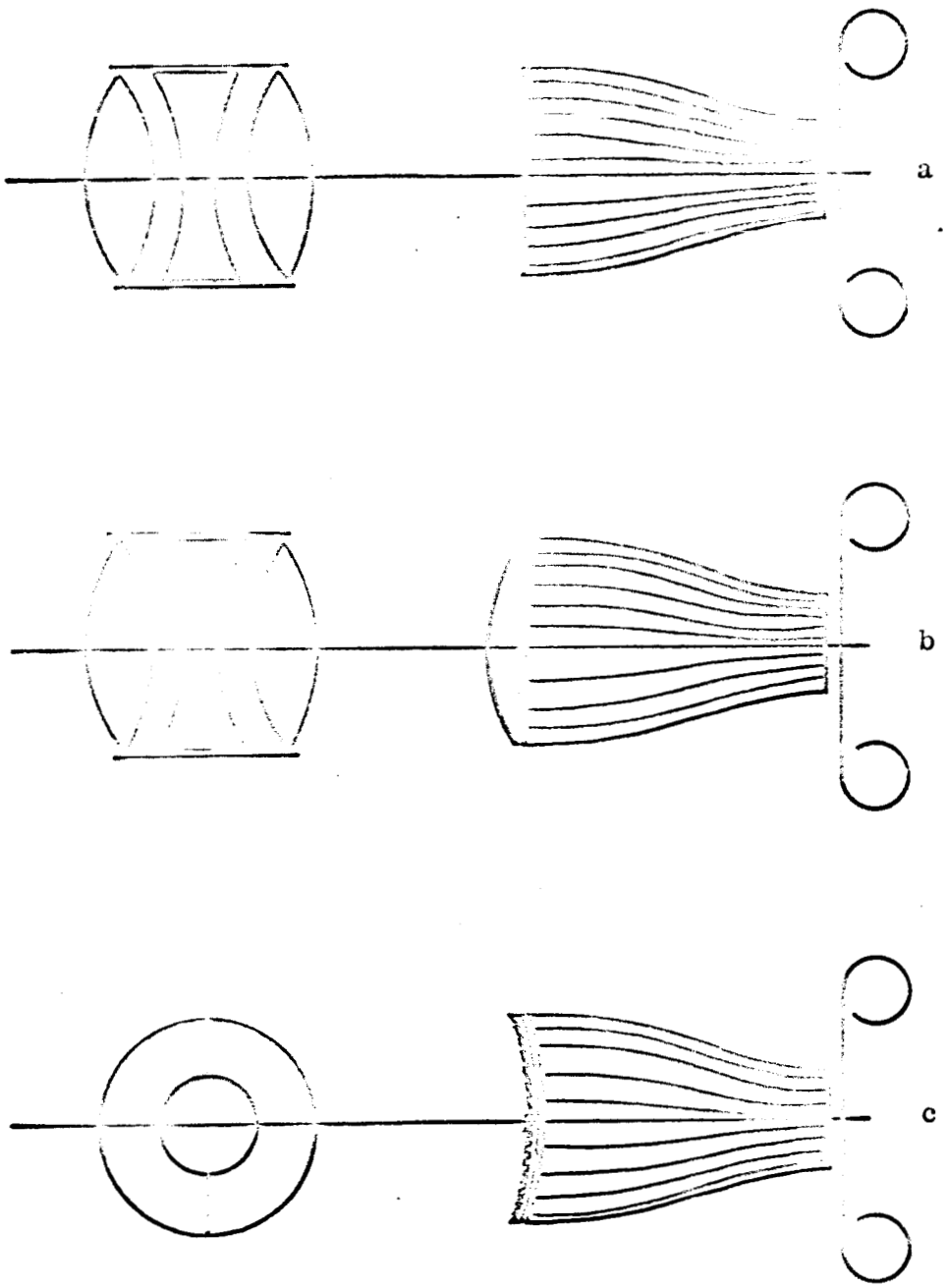

Figure 1 - Typical Lens-Focon Systems

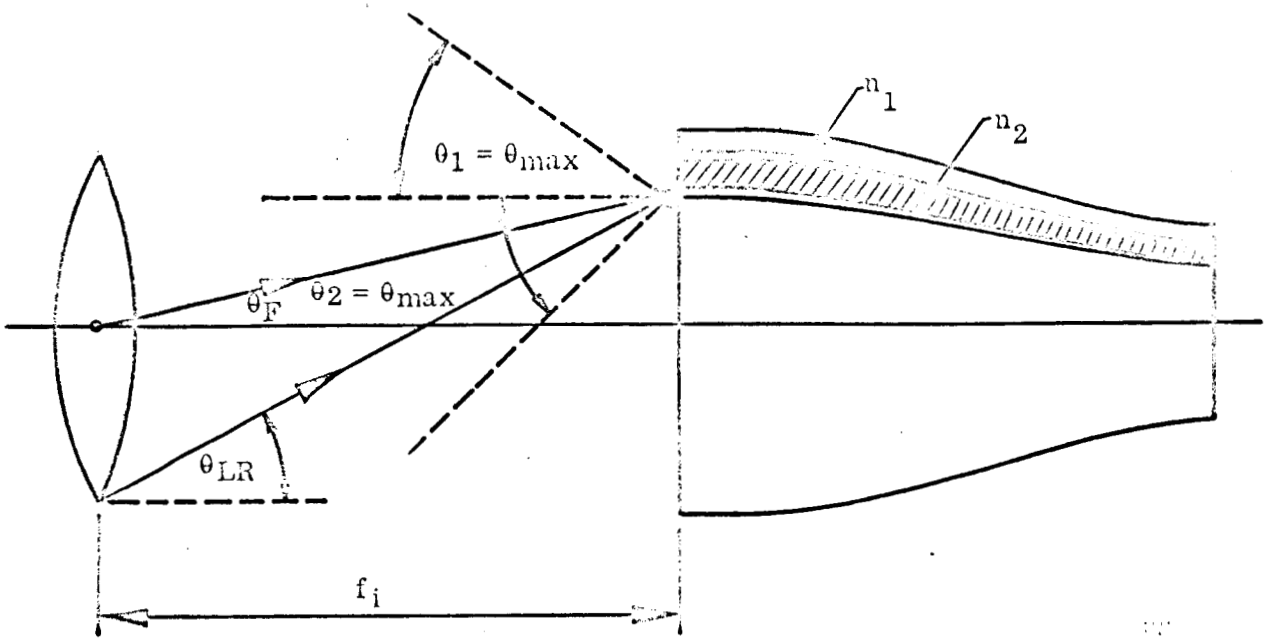

Diameter of objective lens	$= A_i$
Focal length of objective lens	$= f_i$
F/No. of objective lens	$= F_i$
Field angle	$= \theta_F$
Angle which the corresponding lower rim ray makes with the optical axis	$= \theta_{LR}$
Diameter of Focon, input	$= D_1$
Diameter of Focon, output	$= D_2$
Maximum angle of incidence transmitted without attenuation in the conical fibers	$= \theta_{max}$ $(= \theta_1 = \theta_2)$
Refractive index of core glass	$= n_1$
Refractive index of coating glass	$= n_2$
N. A. of fibers	$= \sqrt{n_1^2 - n_2^2}$

Figure 2 - Optical Schematic of Focon System Parameters

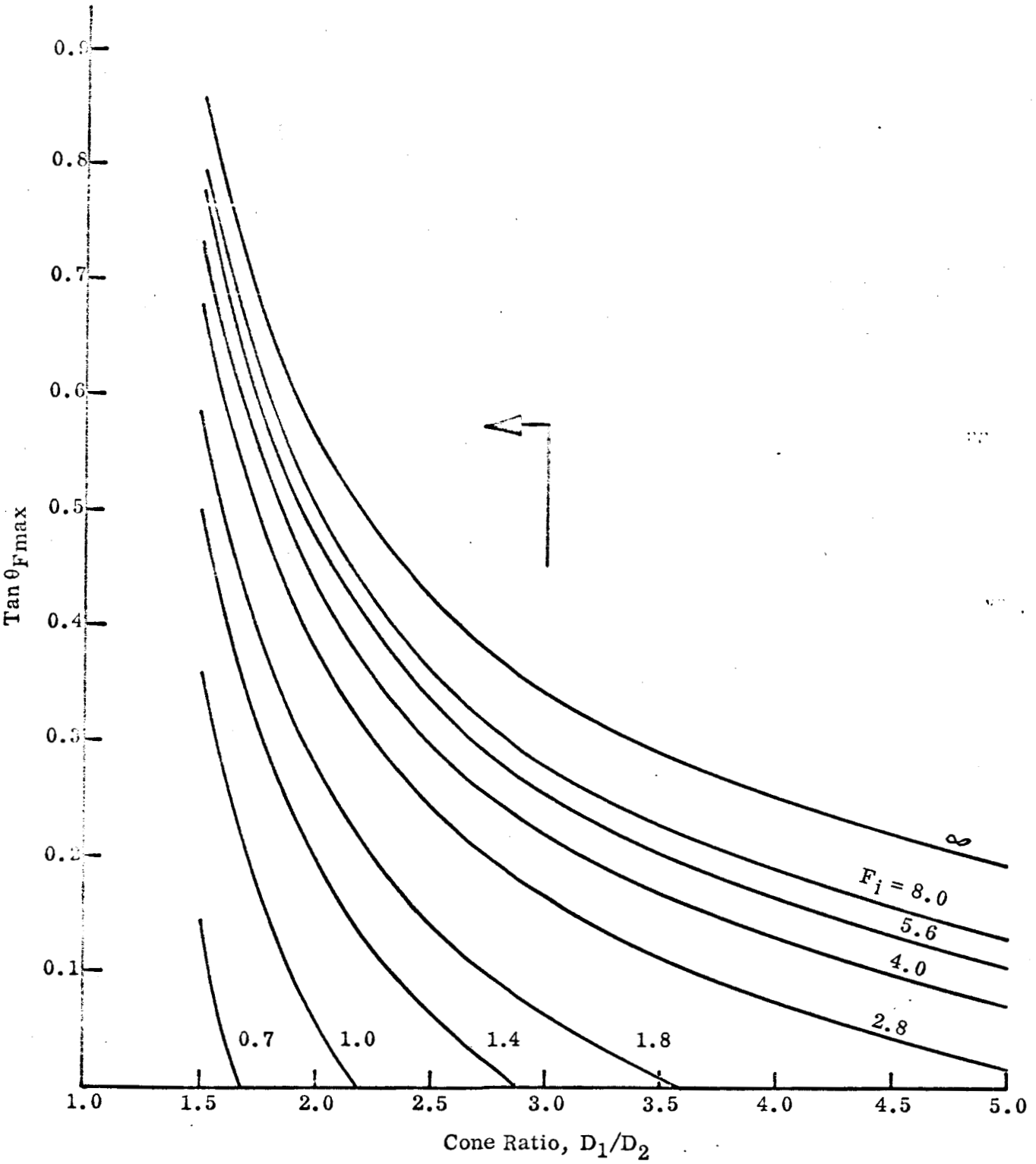

Figure 3 - Variation in Tan θ_{Fmax} as a Function of Cone Ratio for No Vignetting

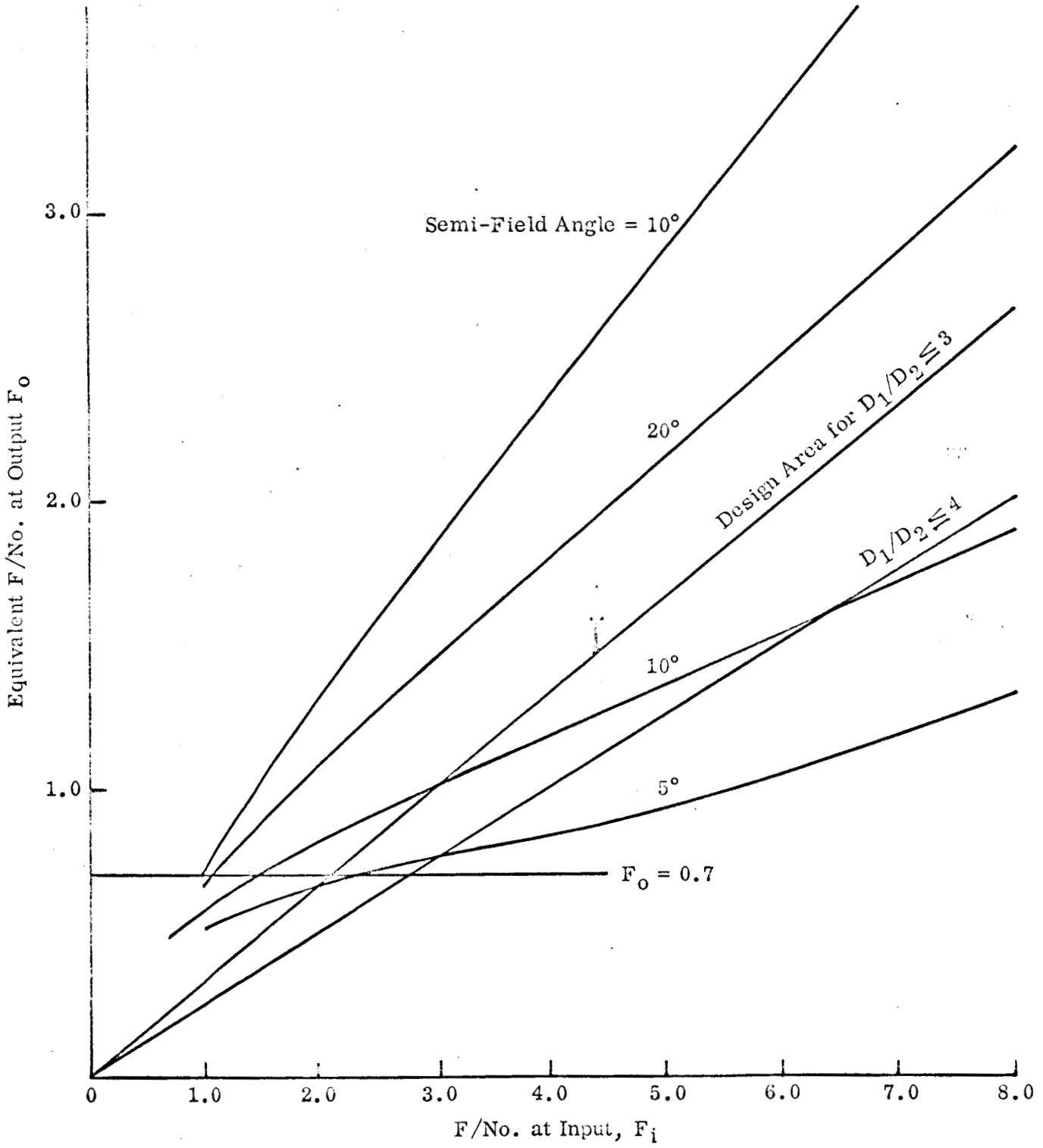

Figure 4 - Minimum Output F/No. Achievable in Focon System as a Function of F/No. of Objective Lens

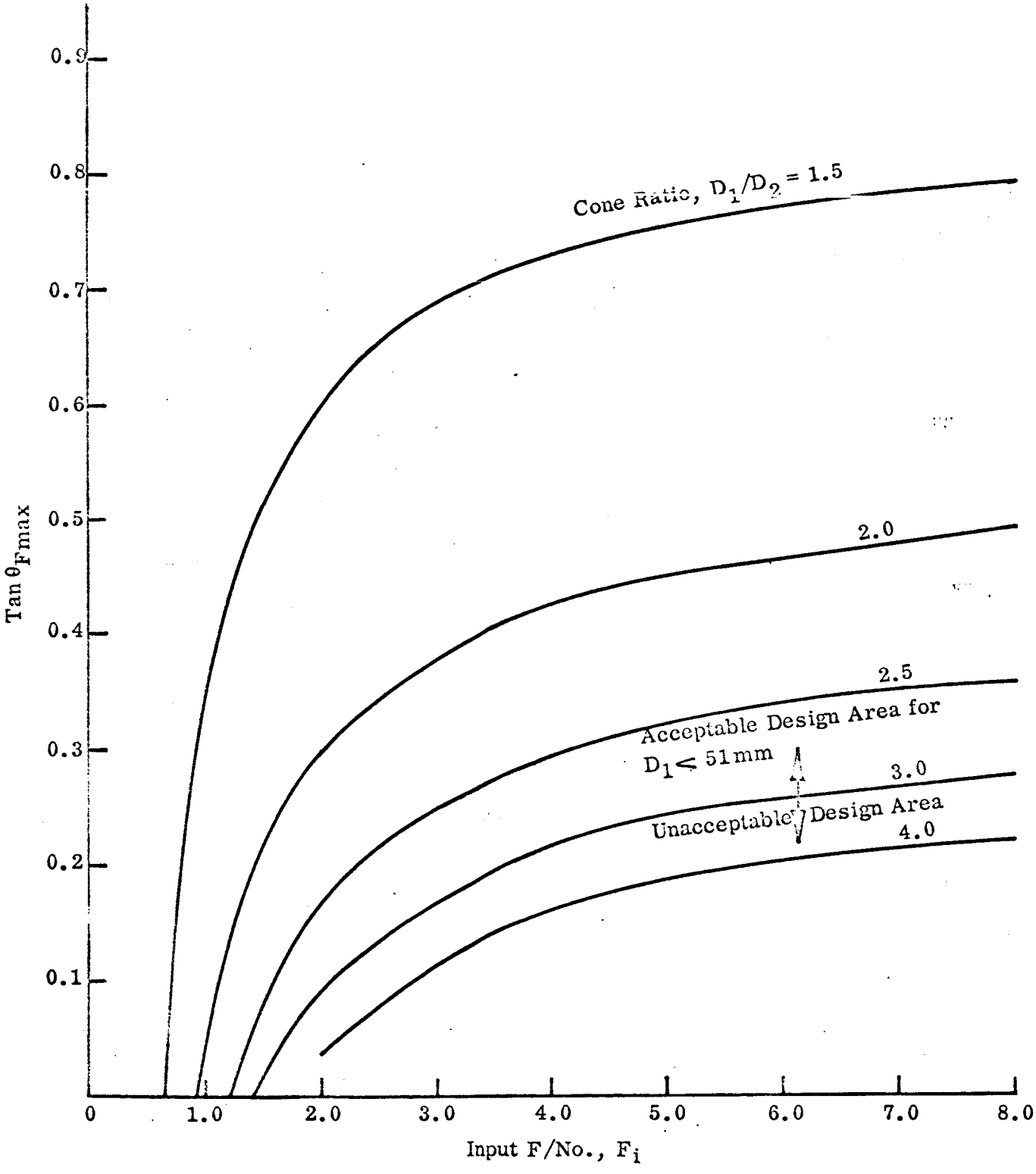

Figure 5 - Variation of Tan θ_{max} as a Function of Input F/No. F_i for No Image Vignetting

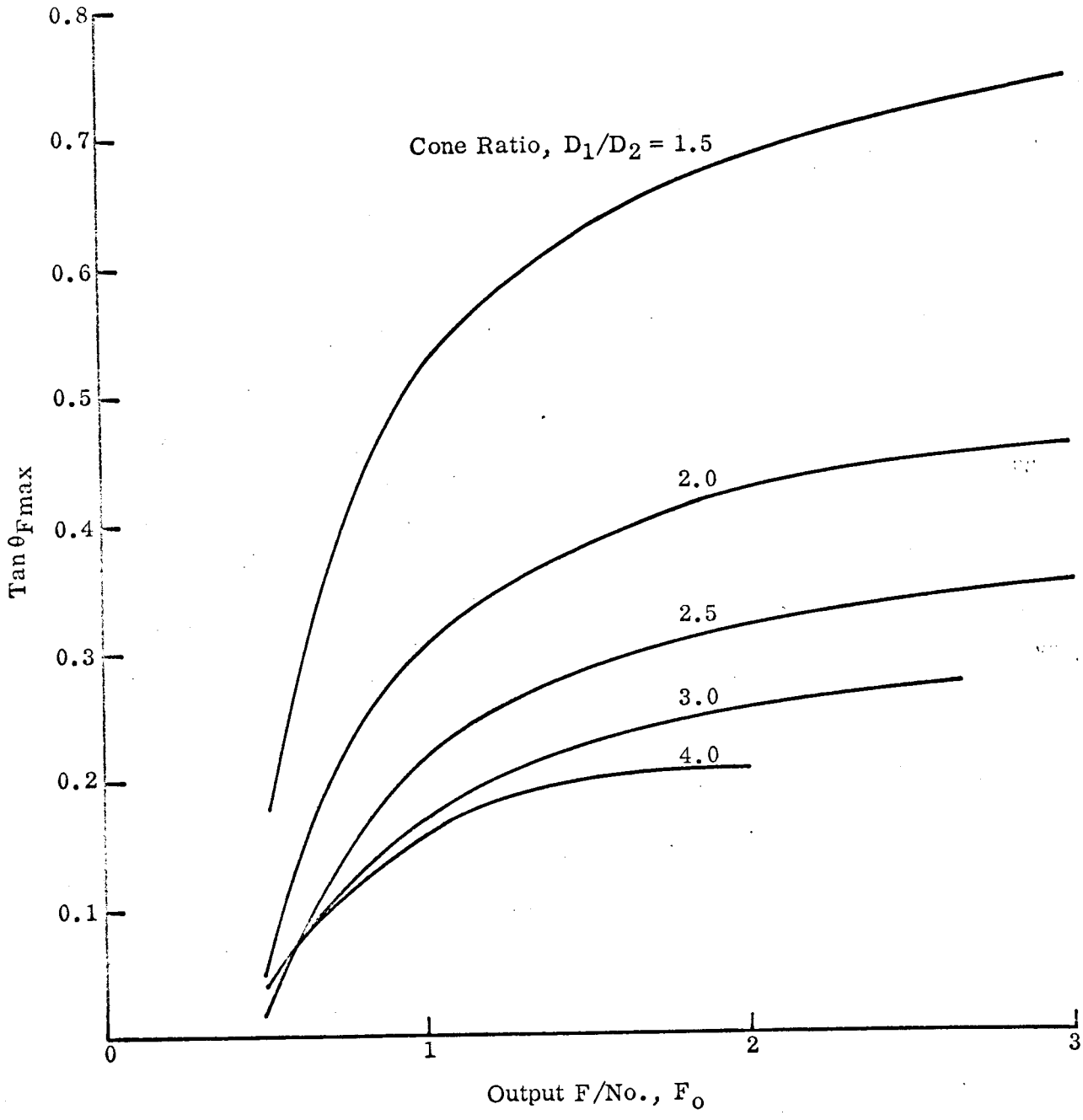

Figure 6 - Variation of Tan θ_{max} as a Function of Output F/No. for No Image Vignetting

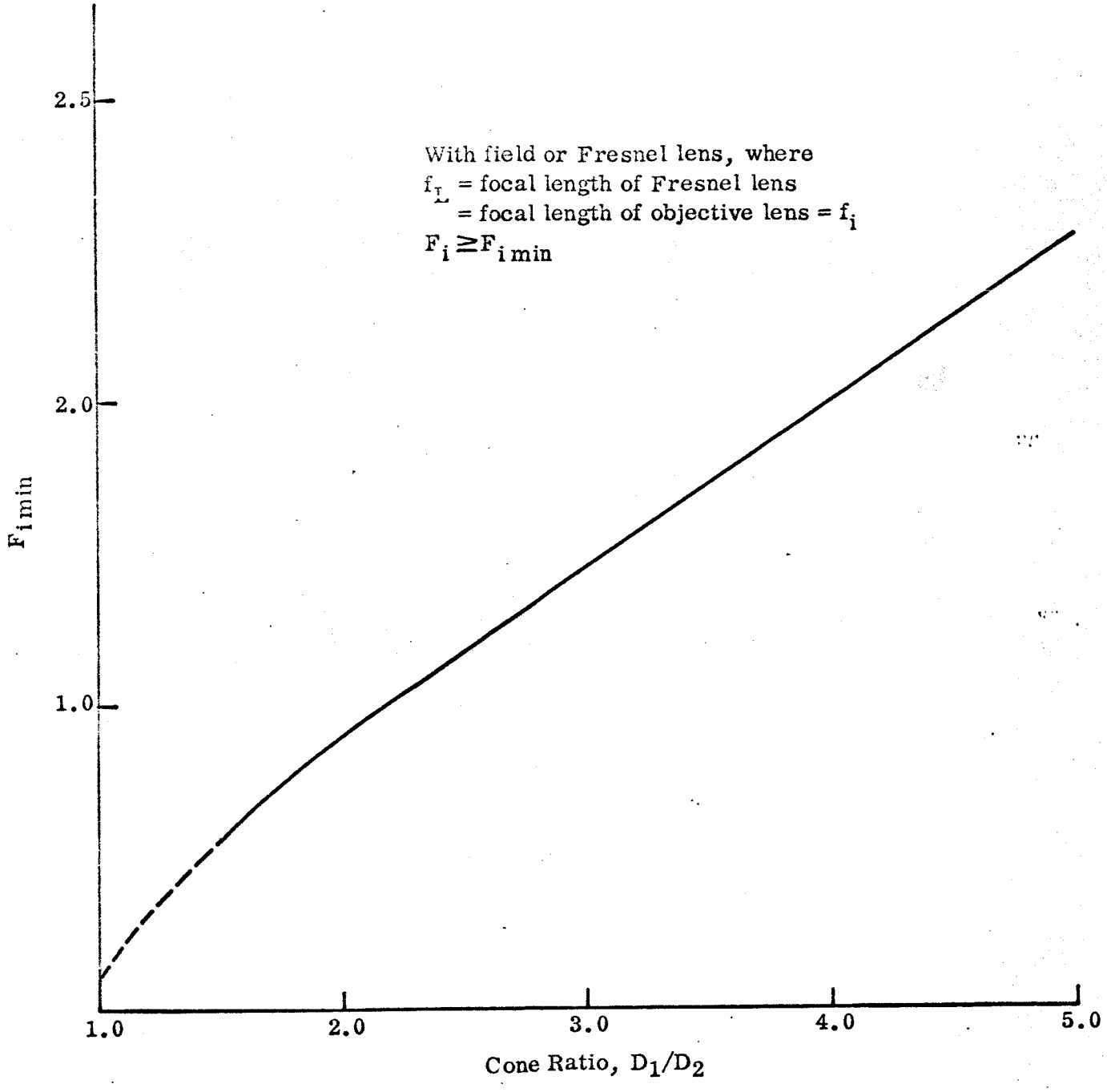

Figure 7 - Minimum Equivalent Output F/No. Achievable as a Function of Cone Ratio of a Field Lens

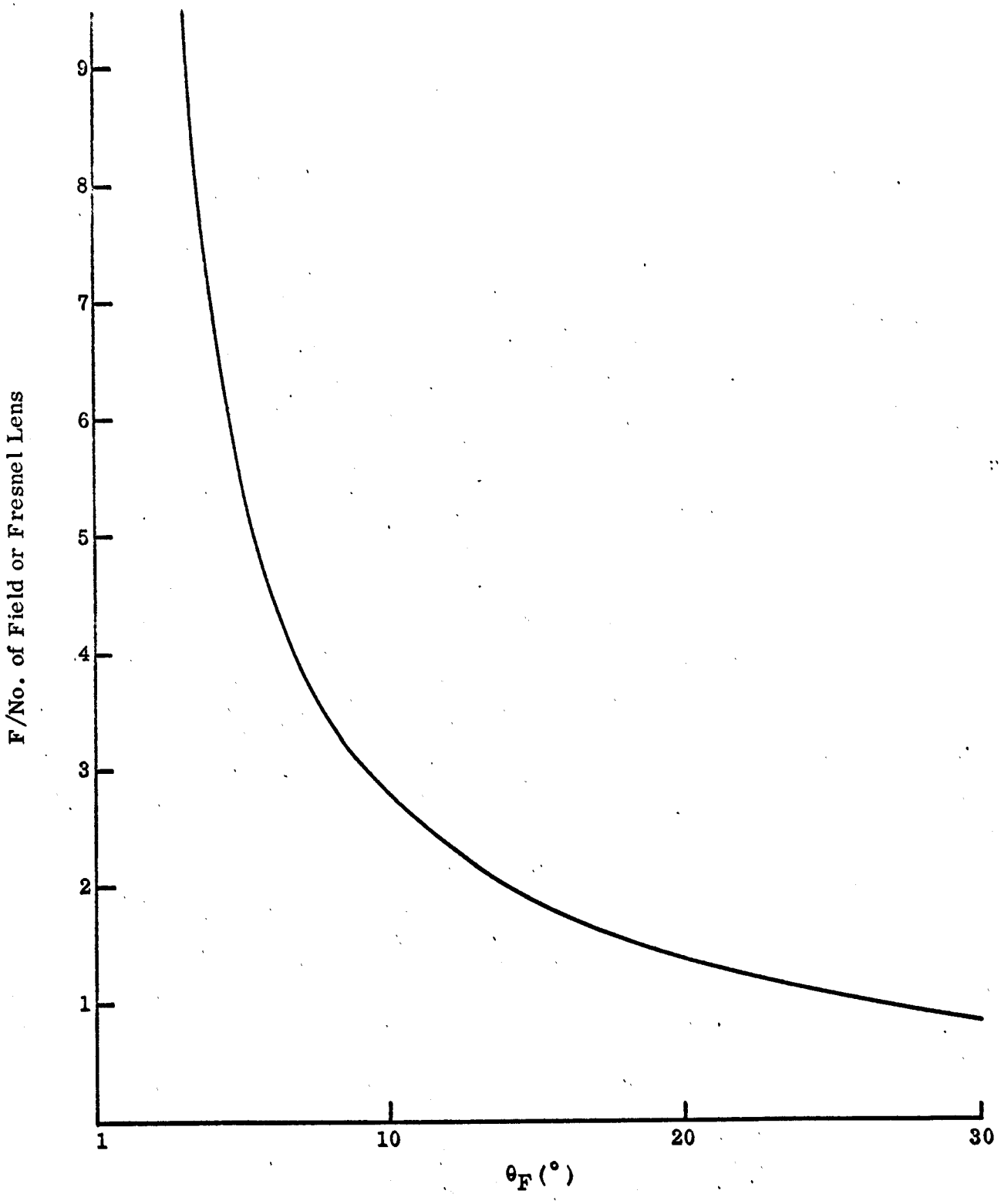

Figure 8 - F/No. of Fresnel or Field Lens for No Meridional Ray Vignetting

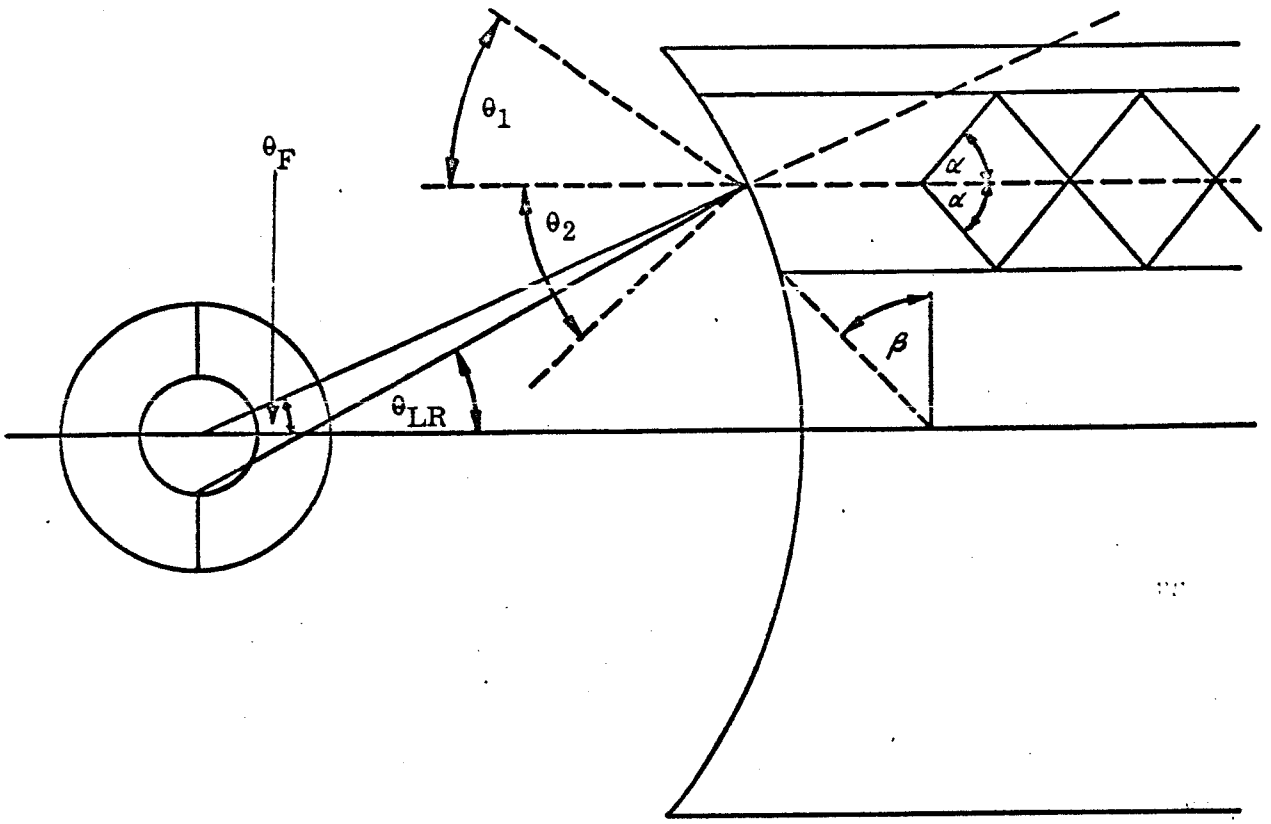

Figure 9 - Ray Trace for Analysis of Image Vignetting in Concentric Optical System using a Fiber Optics Field Flattener

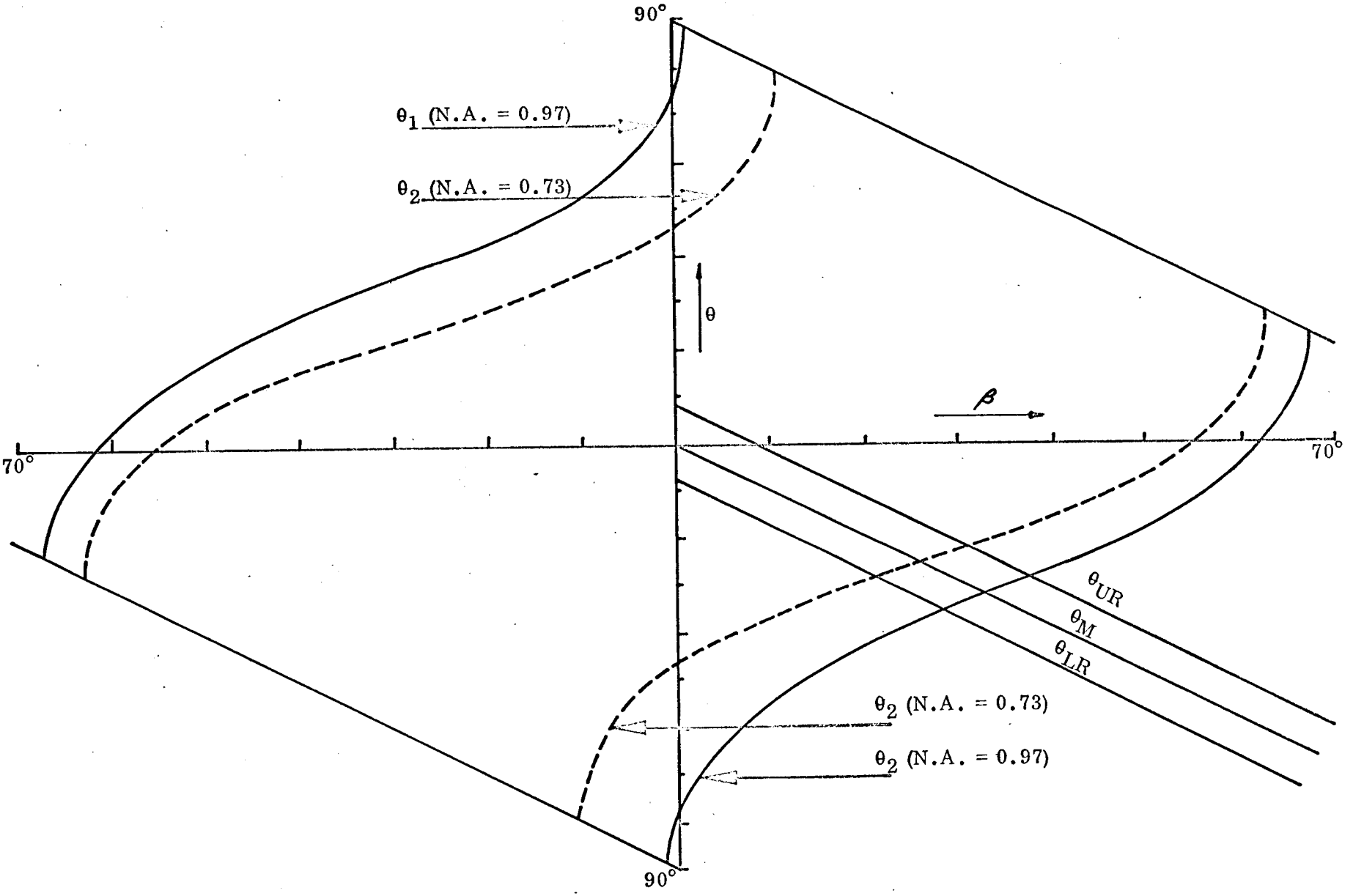

Figure 10 - Plots of Acceptance Angles θ_1 and θ_2 as a Function of Obliquity 0.97 and 0.73 N.A. Fibers

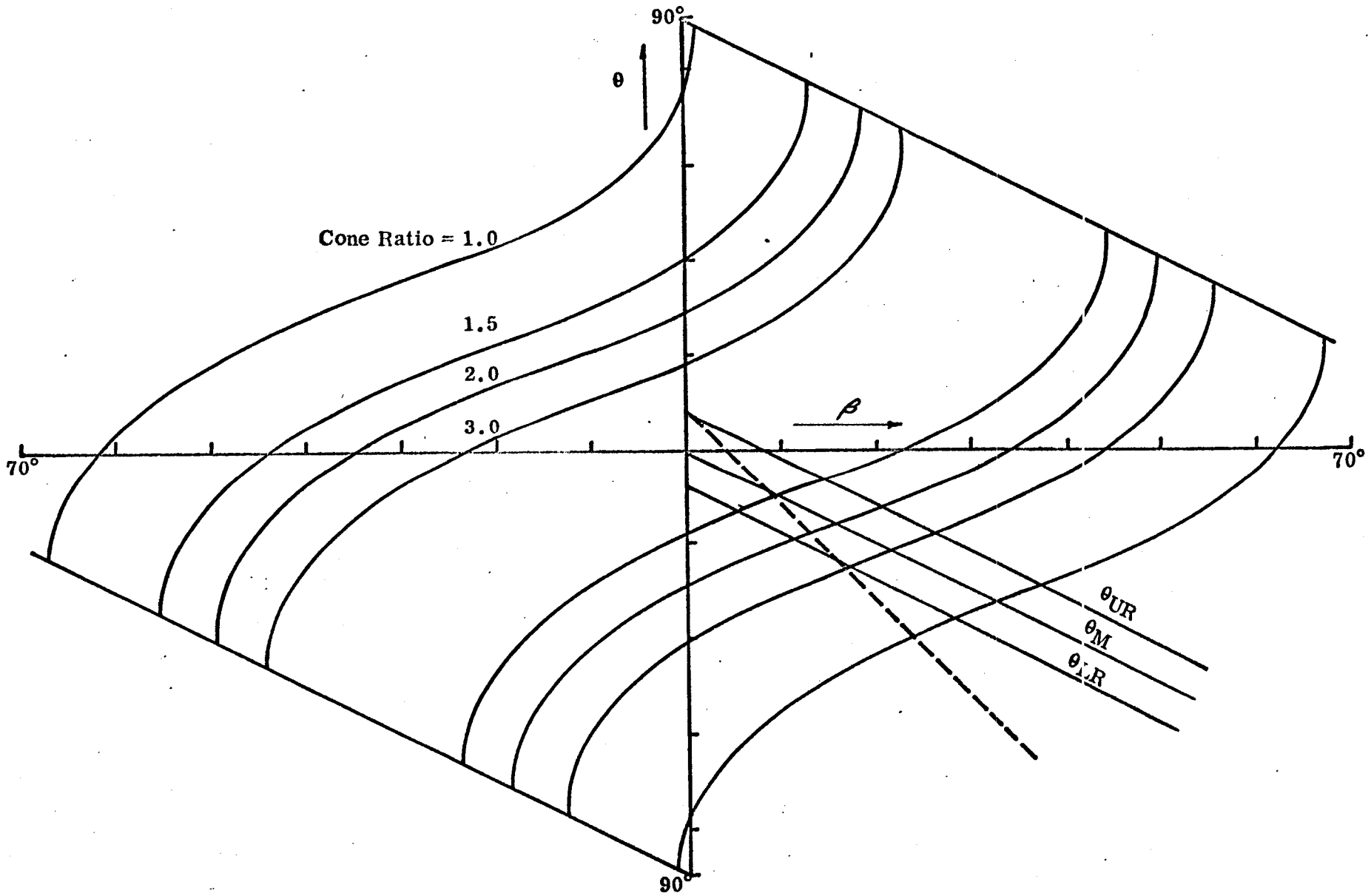

Figure 11 - Plots of Acceptance Angles θ_1 and θ_2 at Several Cone Ratios as a Function of Obliquity of 0.97 N.A. Fibers

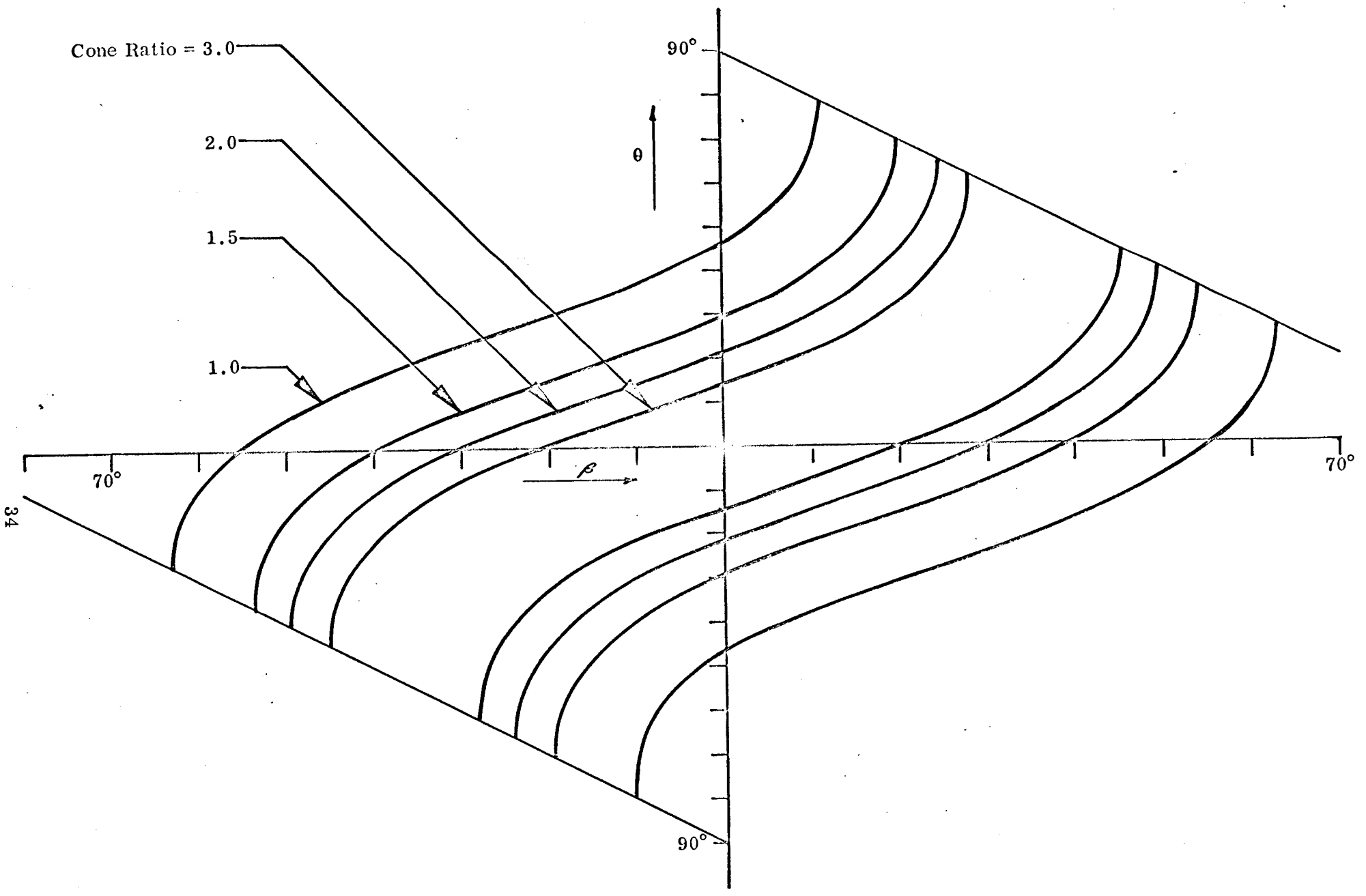

Figure 12 - Plots of Acceptance Angles θ_1 and θ_2 at Several Ratios as a Function of the Obliquity of 0.73 N.A. Fibers

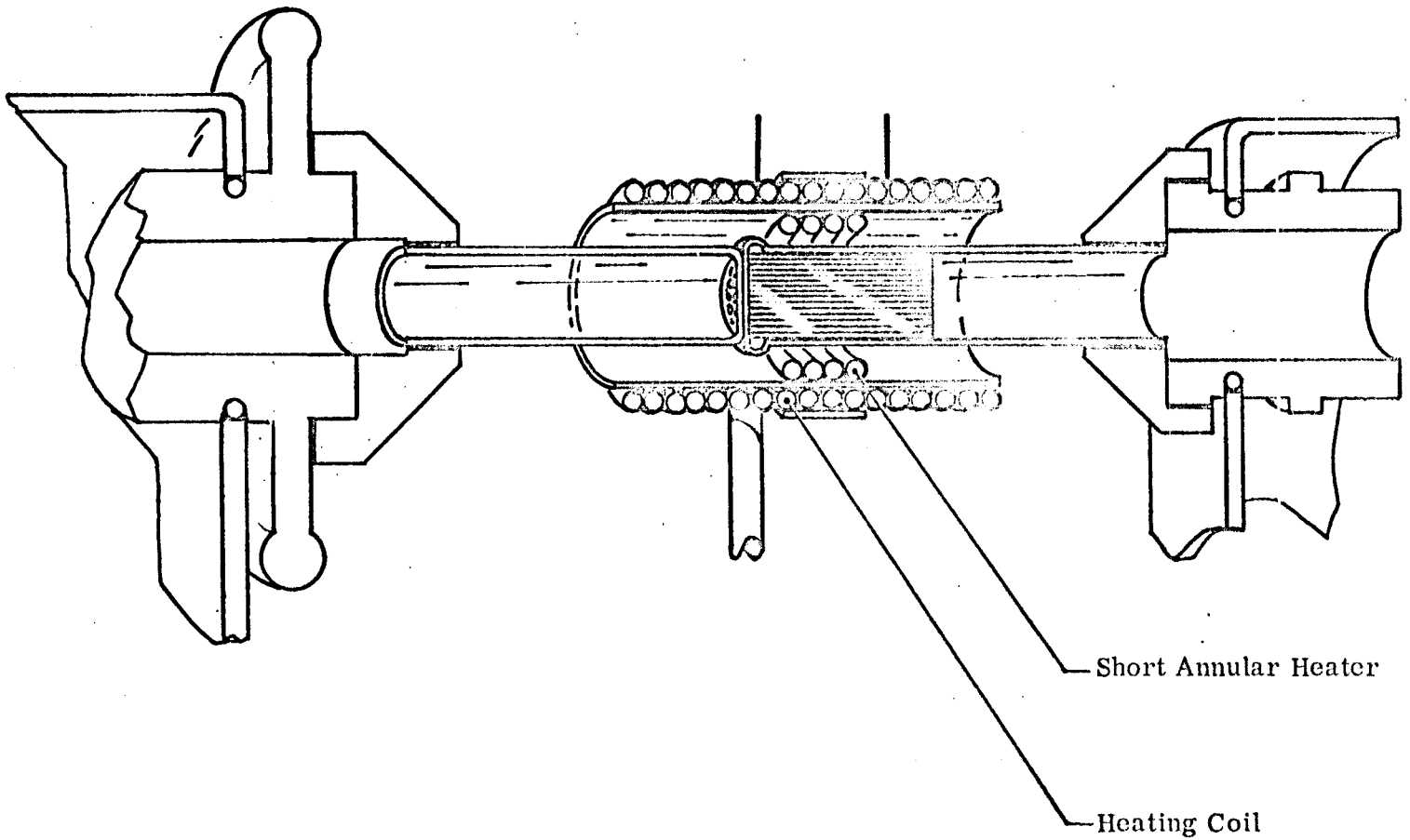

Figure 13 - Schematic of Initial Equipment for Fabricating Focons using a Glass Turner Lathe

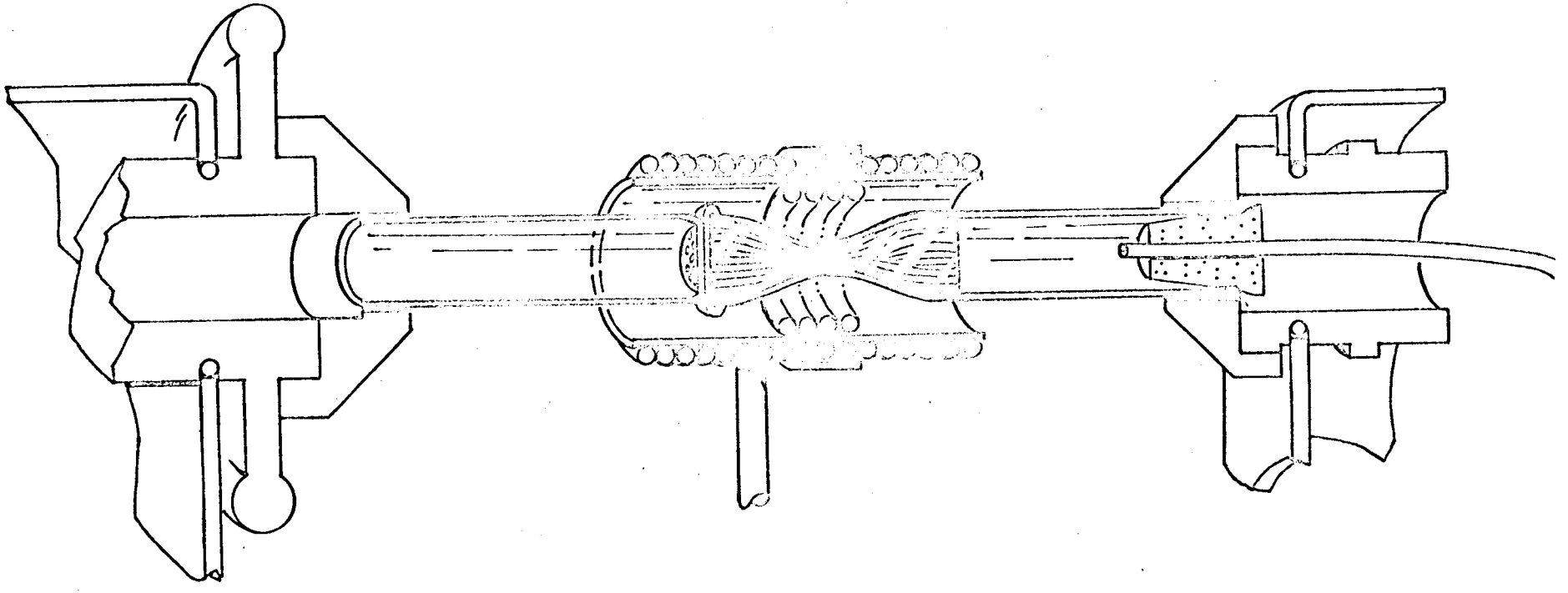

Figure 14 - Schematic of Latest Equipment for Fabricating Focons

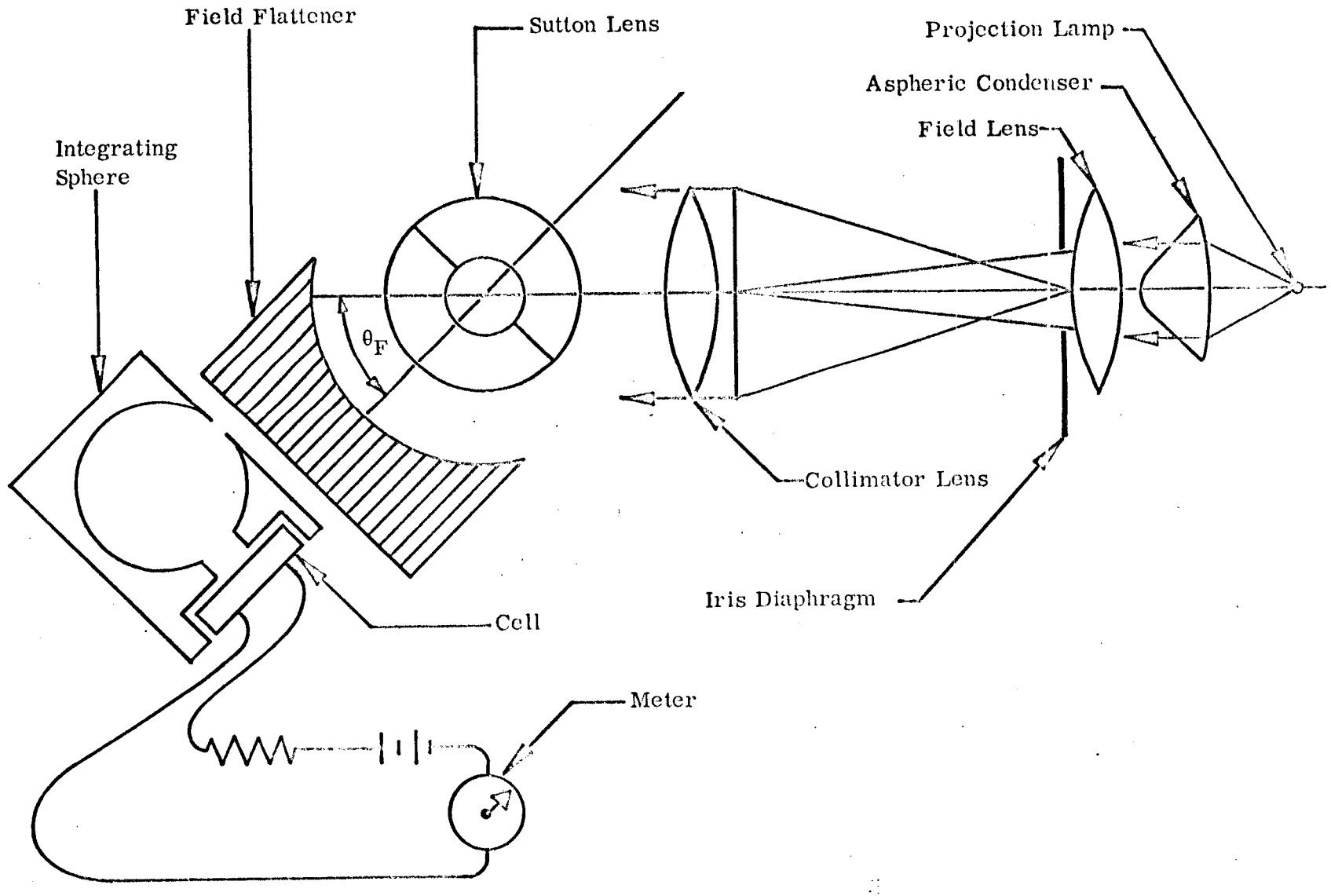

Figure 15 - Schematic of the Apparatus for Vignetting Measurements

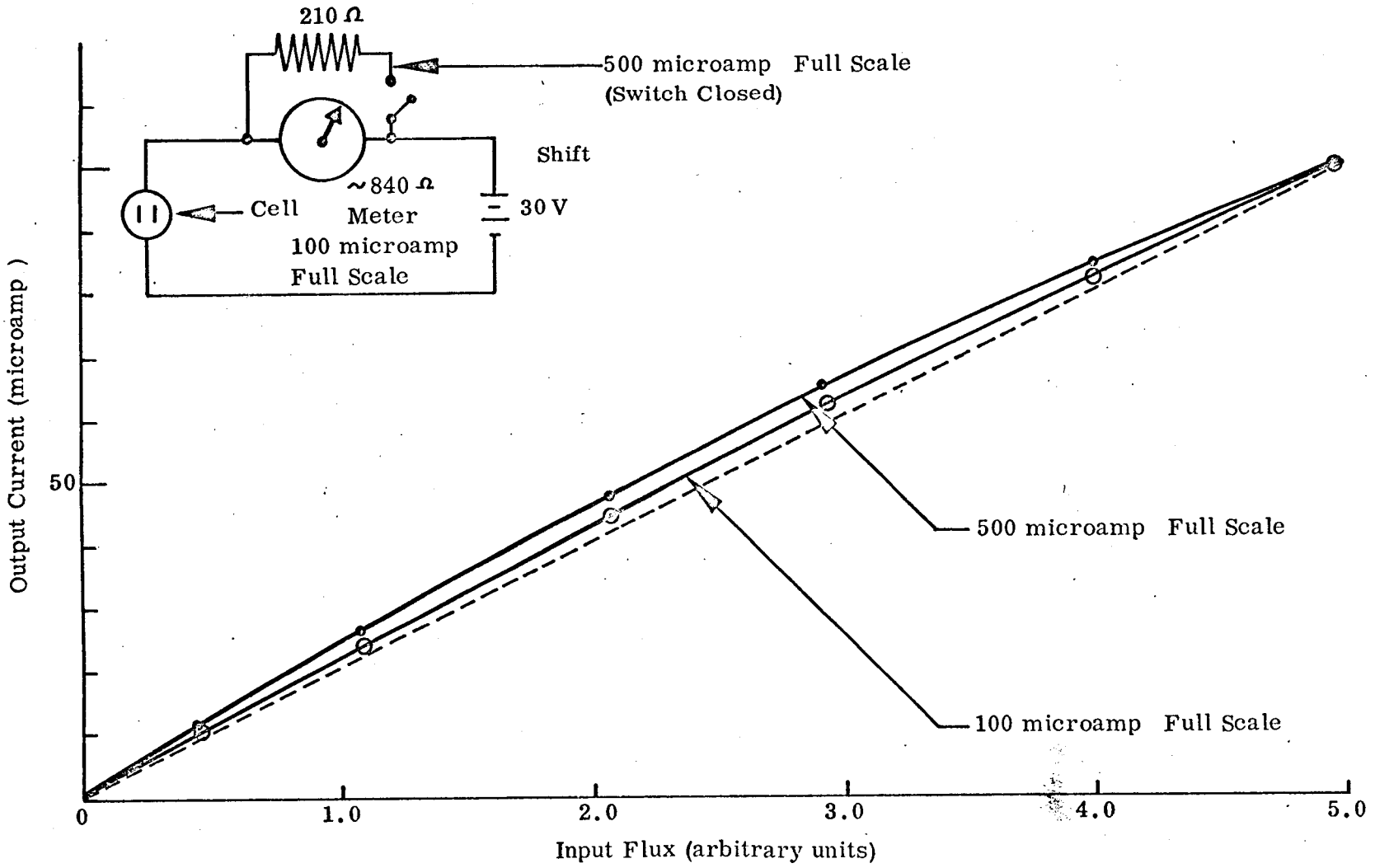

Figure 16 - Calibration Curve for the Cadmium Sulfide Photoconductive Cell and Integrating Sphere used in the Measurements of Image Vignetting

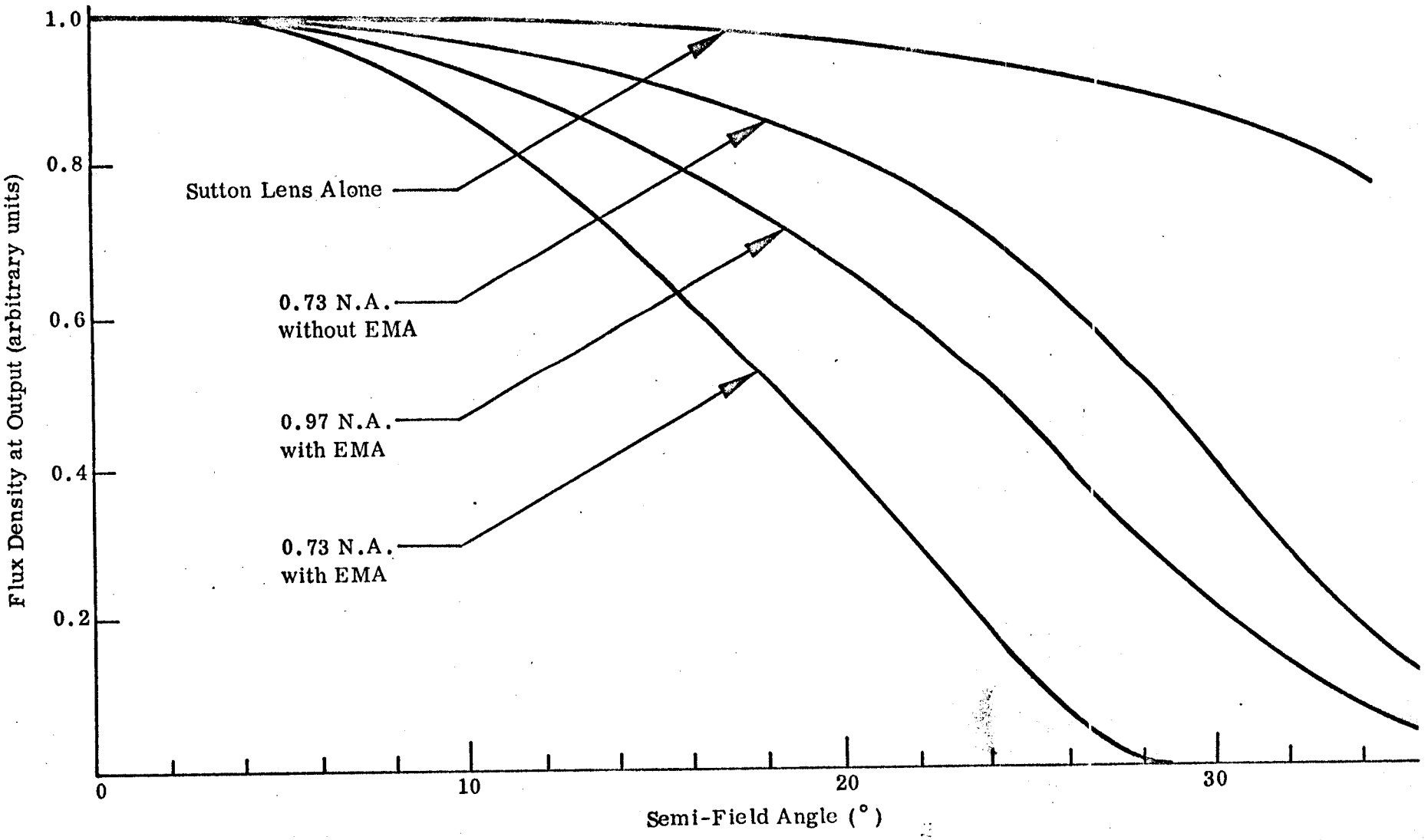

Figure 17 - Vignetting of Field Flattener and Sutton Lens

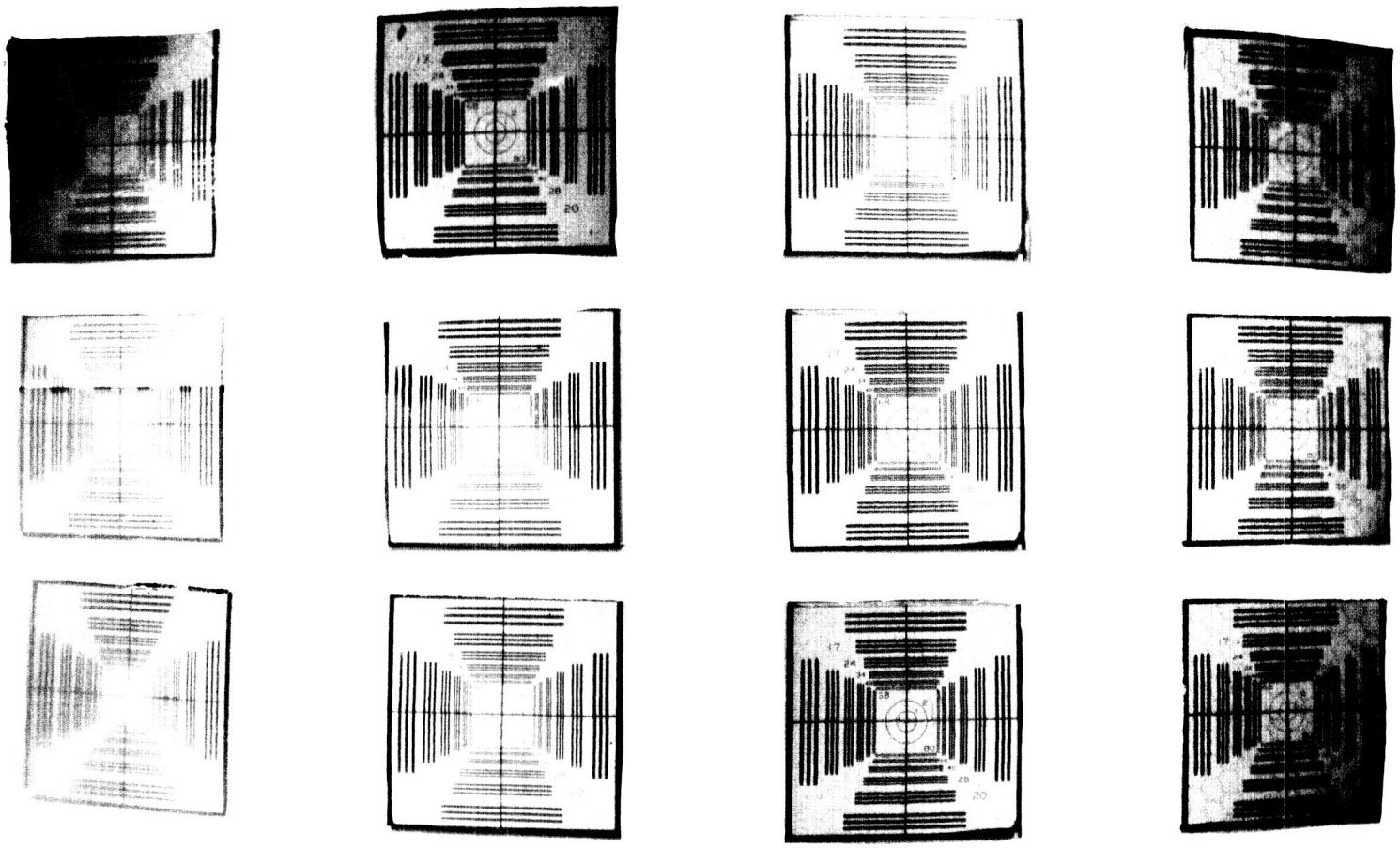

Figure 18 - Photographs of Resolution Charts Taken Through Sutton Lens Camera with a Fiber Optics Field Flattener

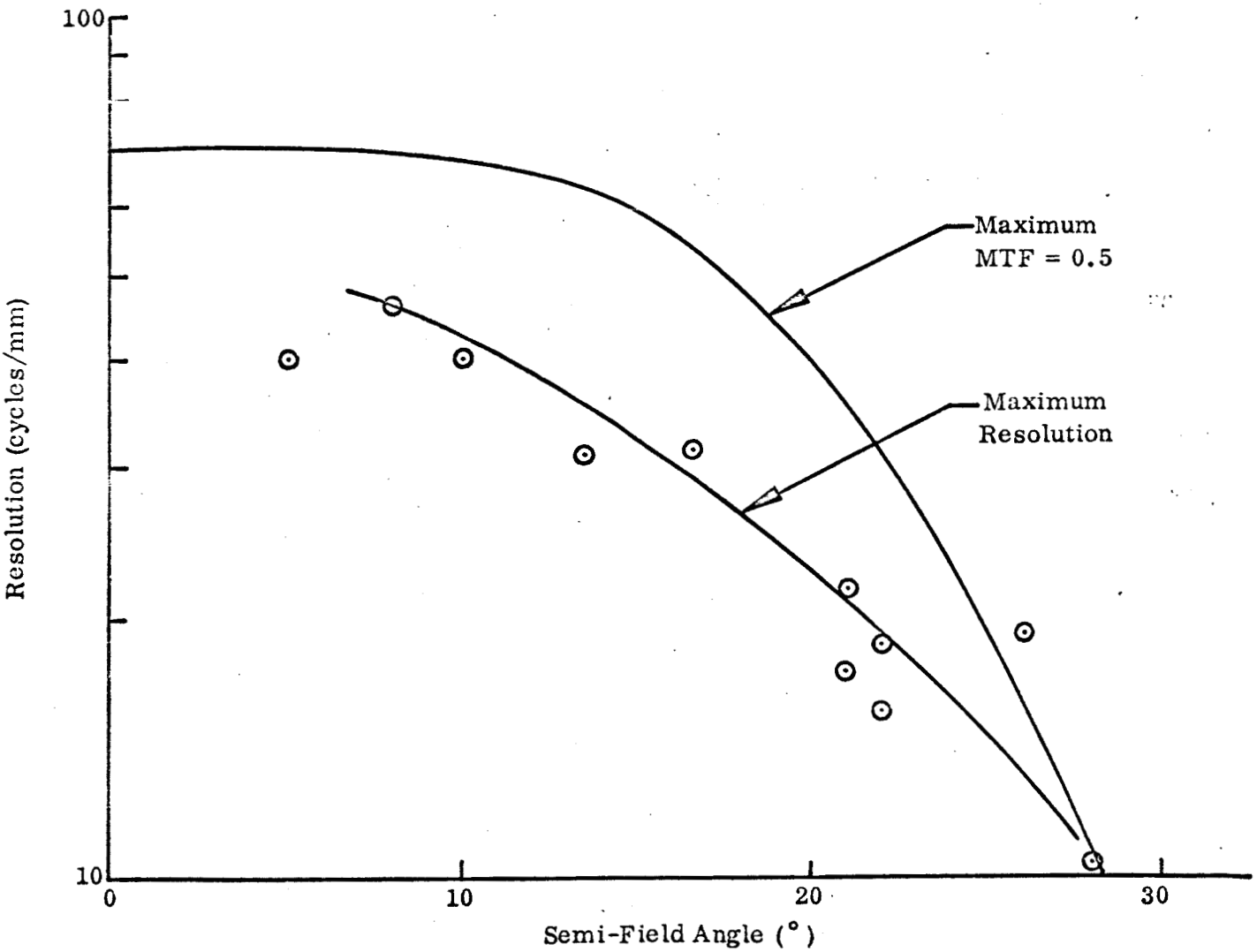

Figure 19 - Photographically Determined Resolution of a Fiber Optics Field Flattener Fabricated from 0.97 N.A., EMA-Coated Fibers

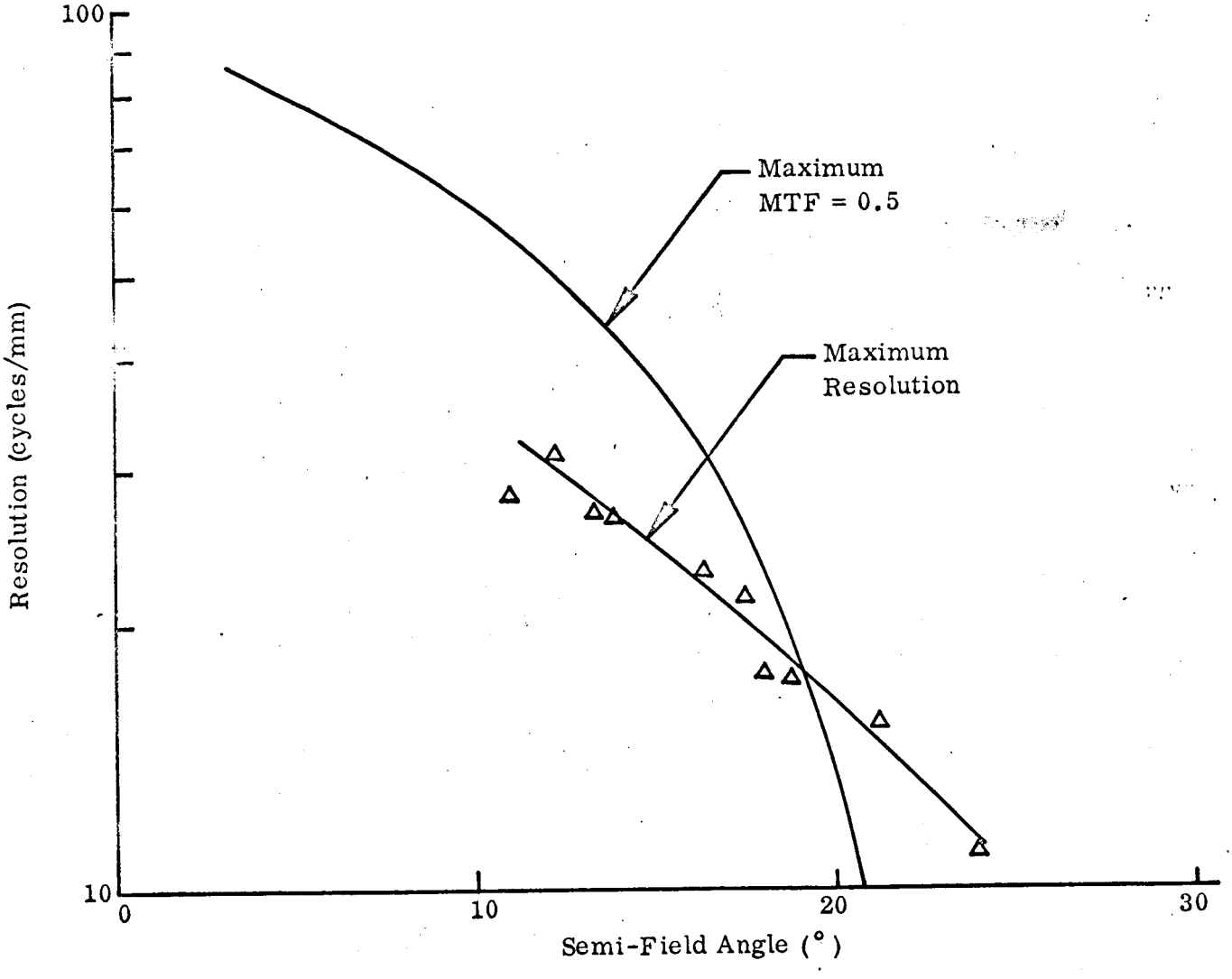

Figure 20 - Photographically Determined Resolution of a Field Flattener Fabricated from 0.73 N.A., EMA-Coated Fibers

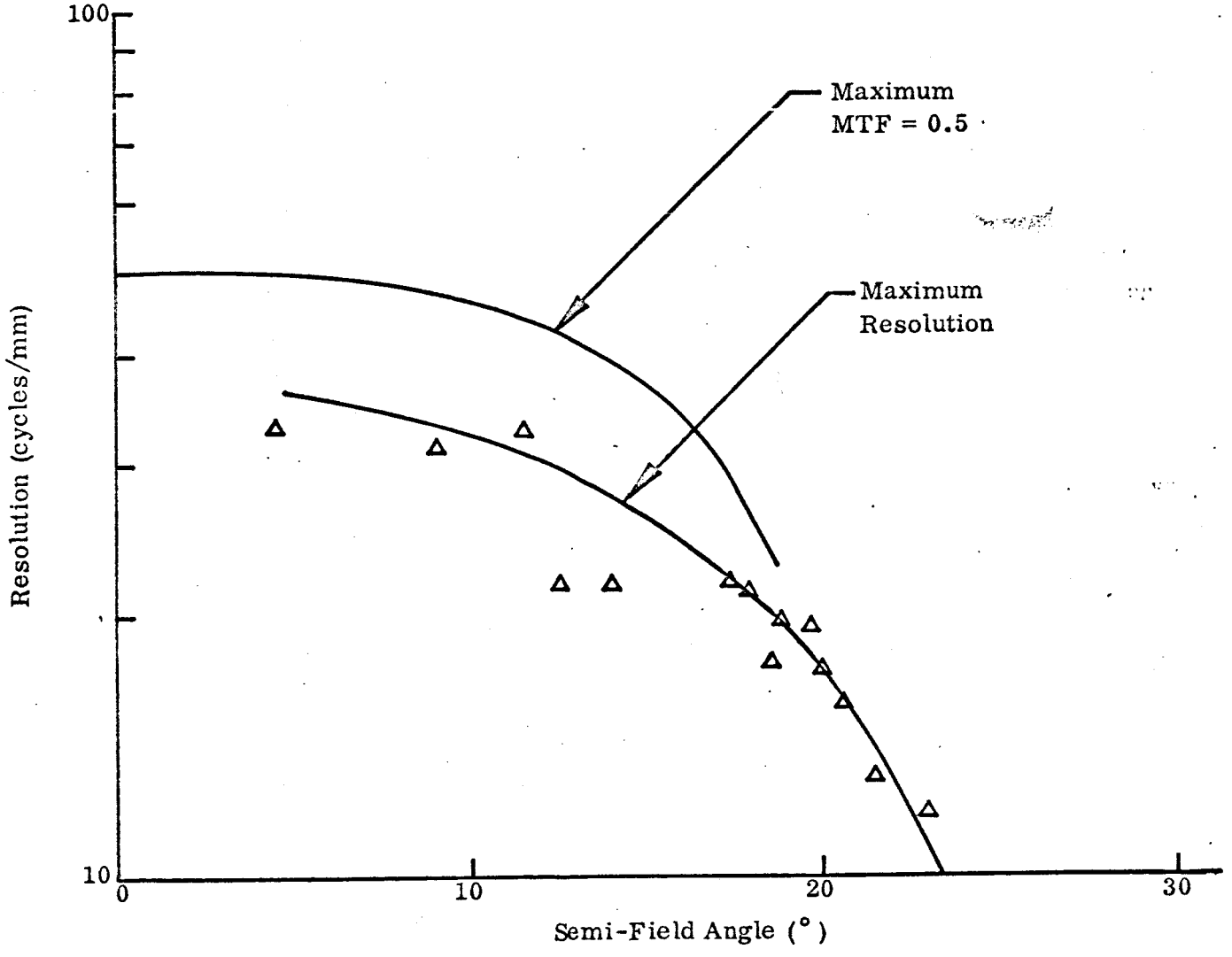

Figure 21 - Photographically Determined Resolution of a Field Flattener Fabricated from 0.73 N.A. Fibers, without EMA Coating

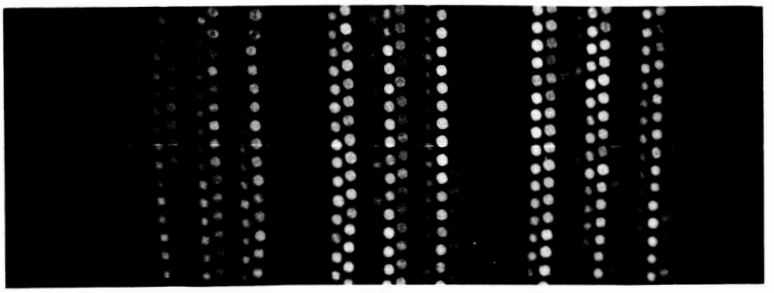

Semi-Field Angle = 3°

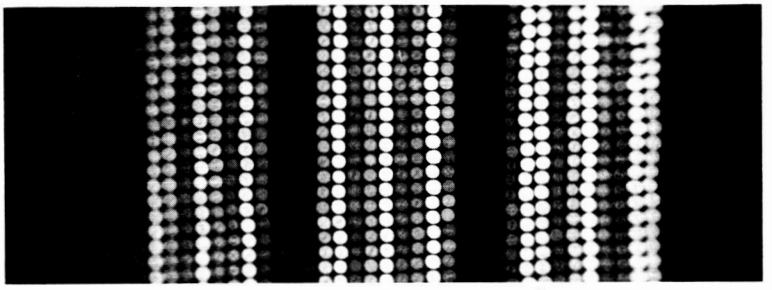

Semi-Field Angle = 8°

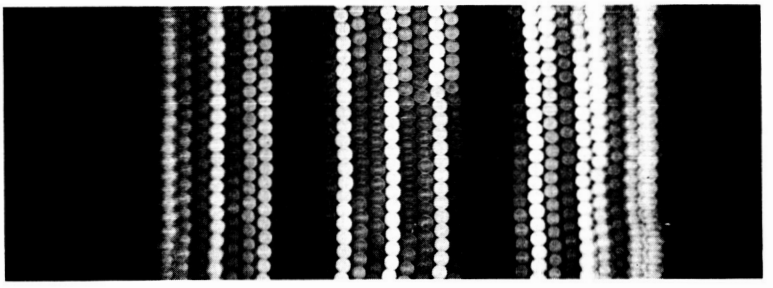

Semi-Field Angle = 16°

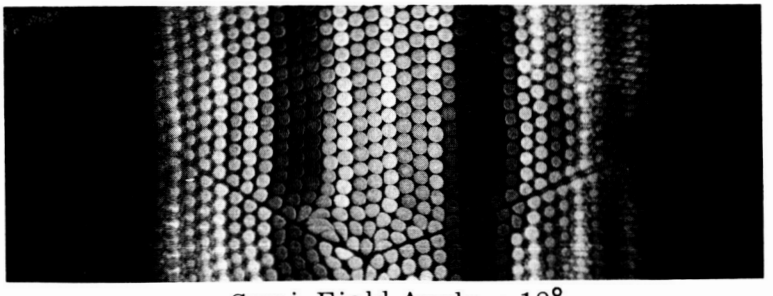

Semi-Field Angle = 18°

Figure 22 - Photographs of a Bar Chart Taken Through the Sutton Camera with a Field Flattener Fabricated from 0.73 N.A. Fibers, without EMA Coating

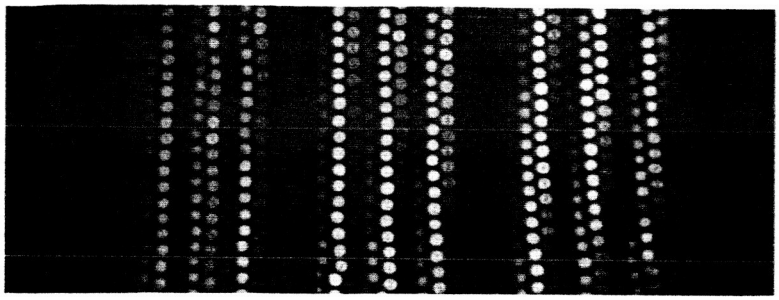

Semi-Field Angle = 3°

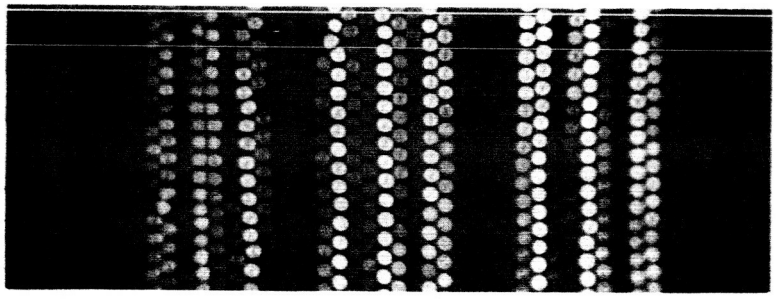

Semi-Field Angle = 8°

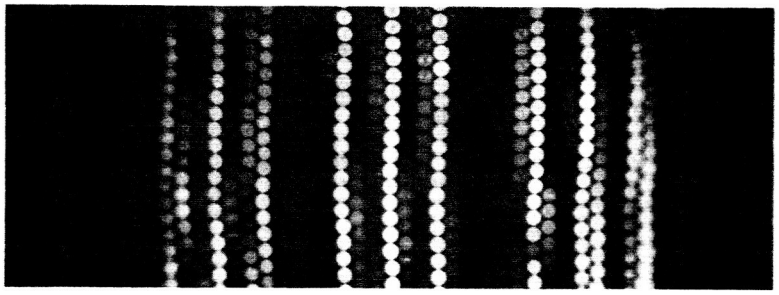

Semi-Field Angle = 16°

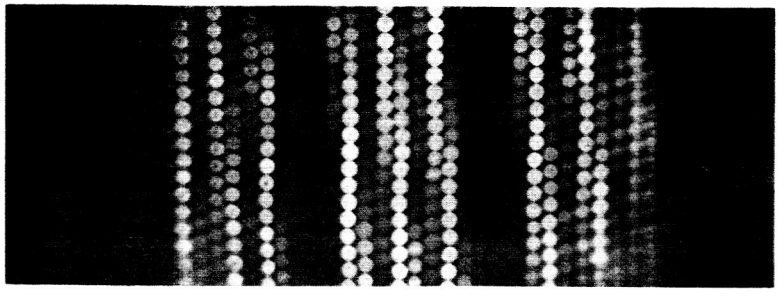

Semi-Field Angle = 18°

Figure 23 - Photographs of a Bar Chart Taken Through the Sutton Camera with a Field Flattener Fabricated from 0.96 N.A., EMA-Coated Fibers

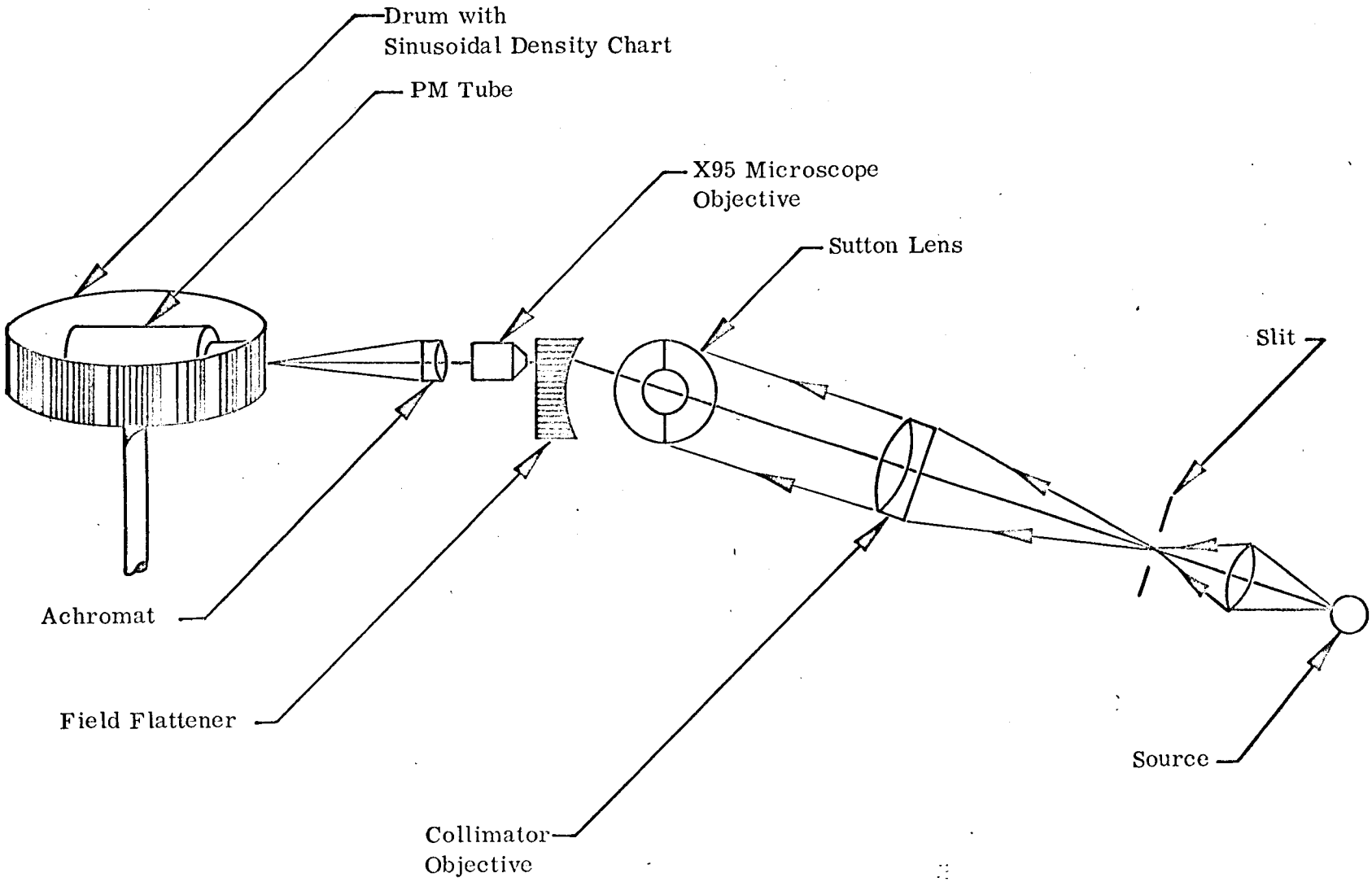

Figure 24 - Schematic of MTF Measuring Equipment

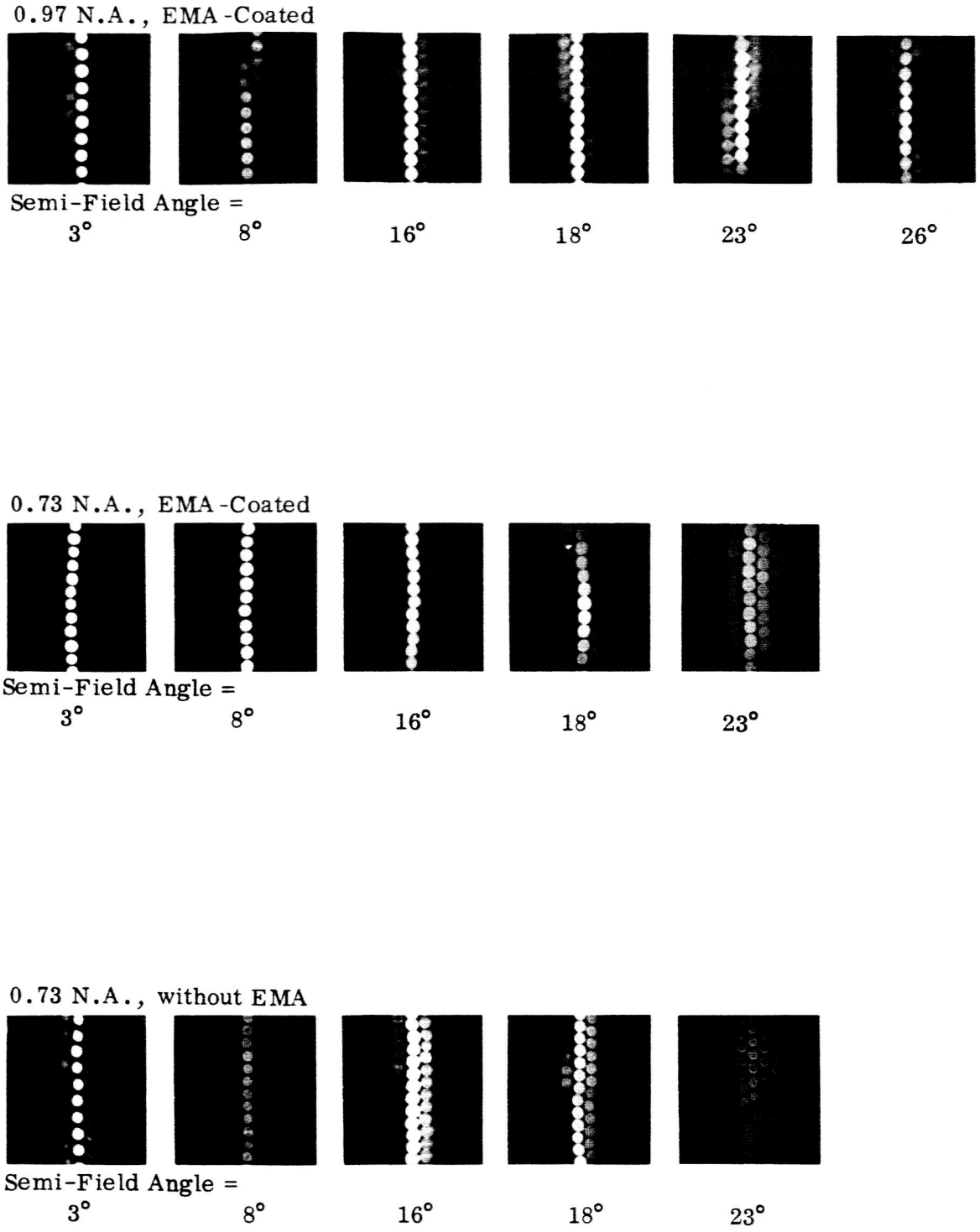

Figure 25 - Photographs of Field Flattener Line Spread Functions at Several Field Angles

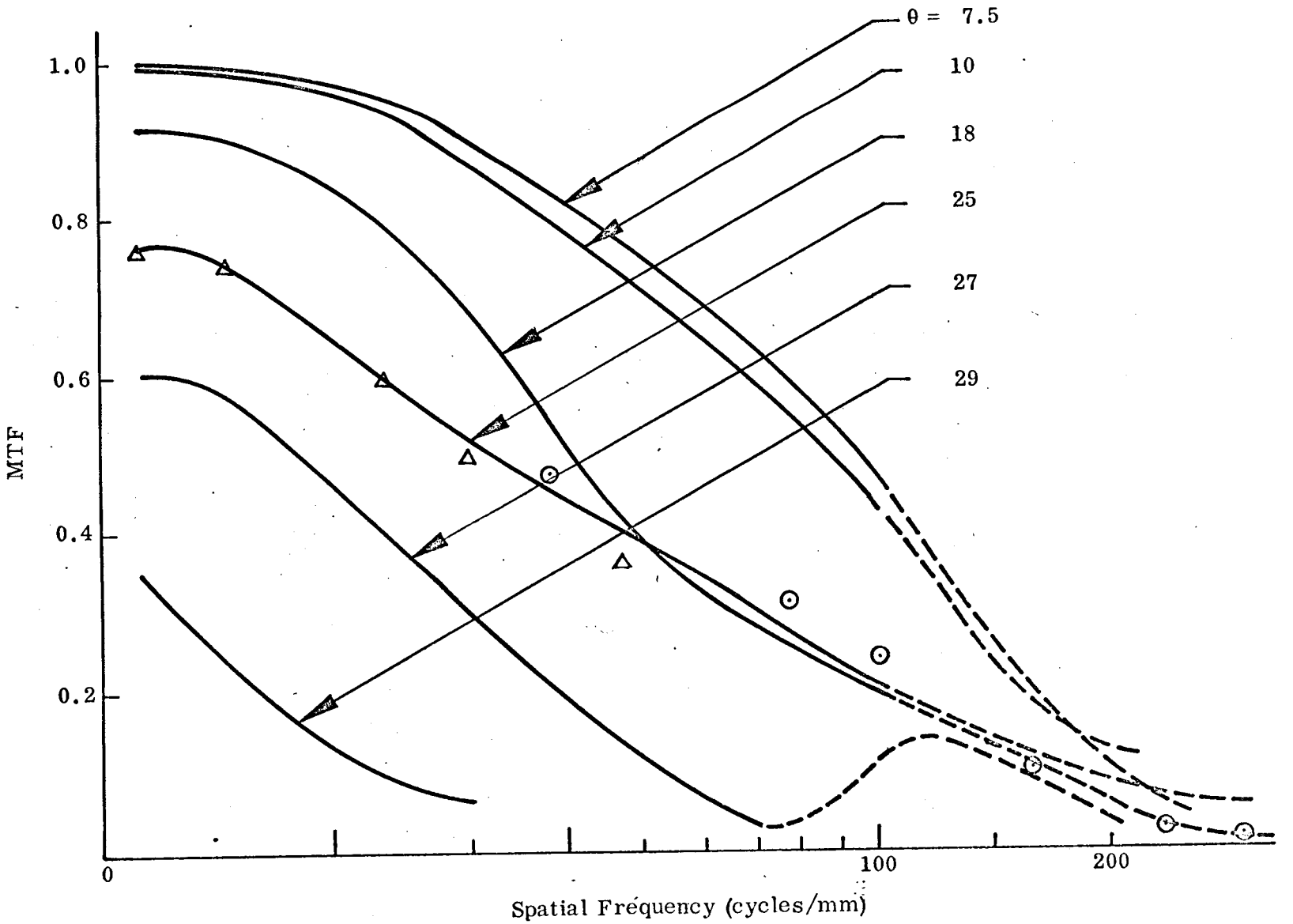

Figure 26 - MTF of Sutton Lens Camera with Field Flattener Fabricated from 0.97 N.A., EMA-Coated Fibers

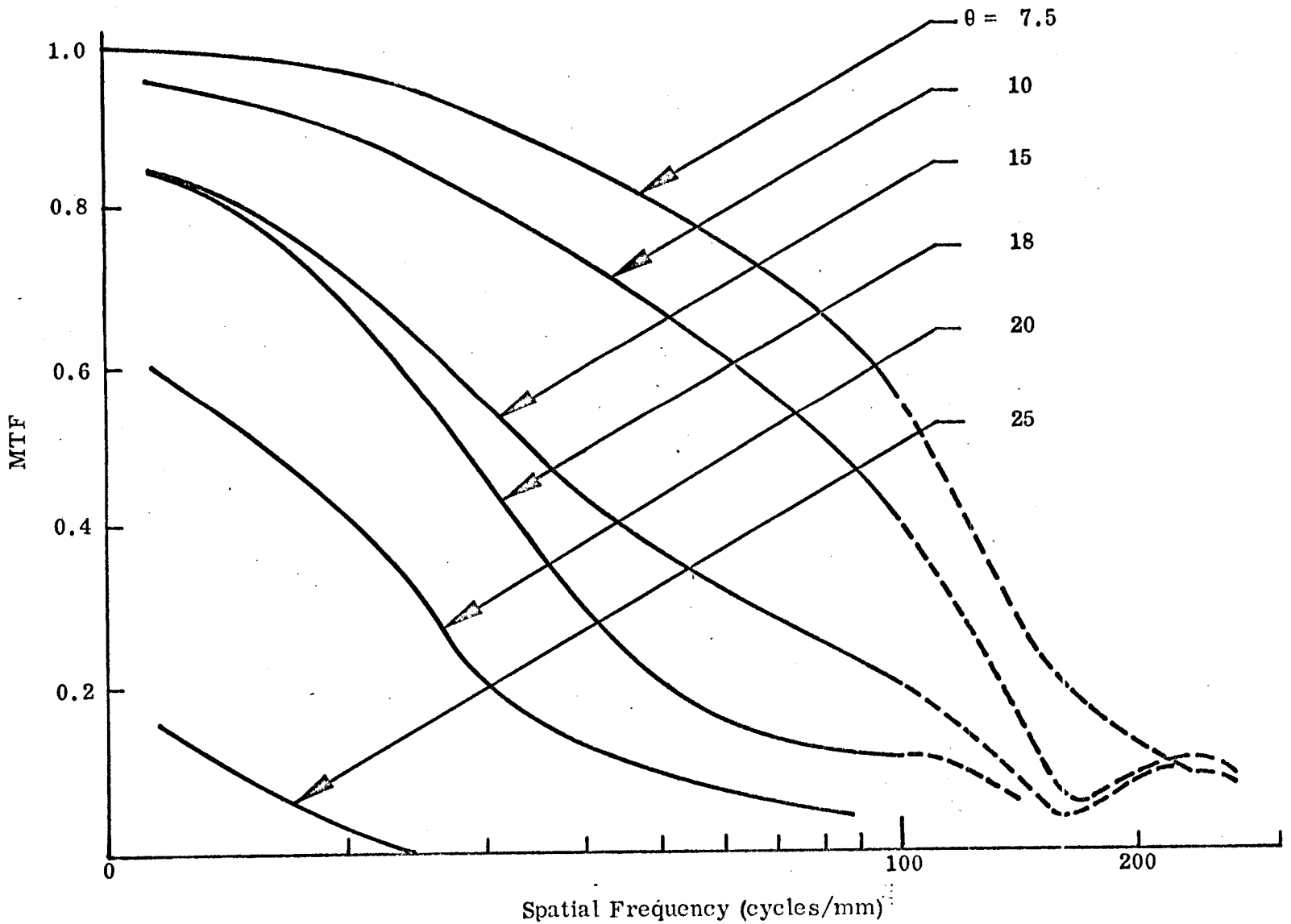

Figure 27 - MTF of Sutton Lens Camera with Field Flattener Fabricated from 0.73 N.A., EMA-Coated Fibers

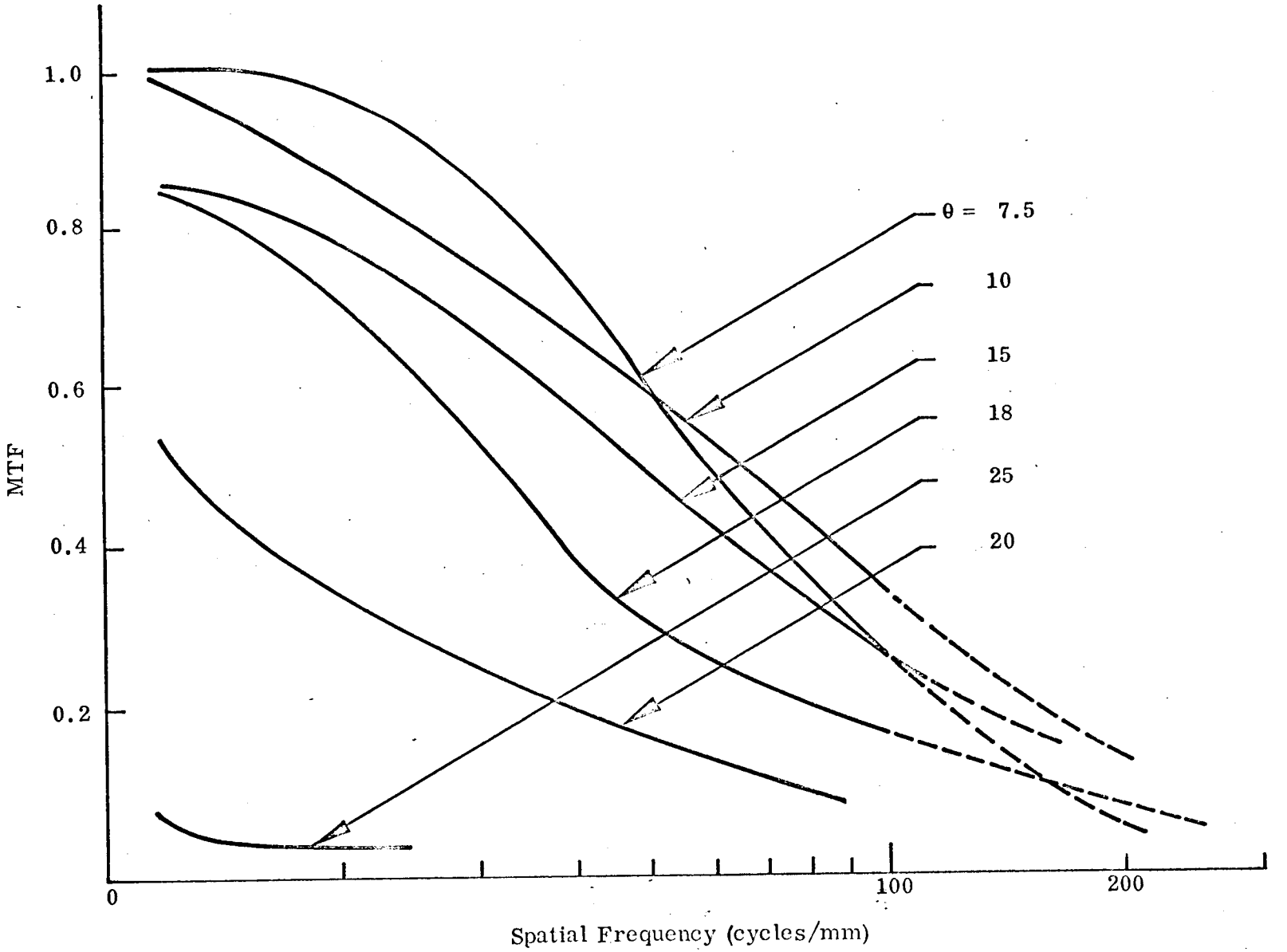

Figure 28 - Sutton Lens Camera with Field Flattener Fabricated from 0.73 N.A. Fibers, without EMA Coating

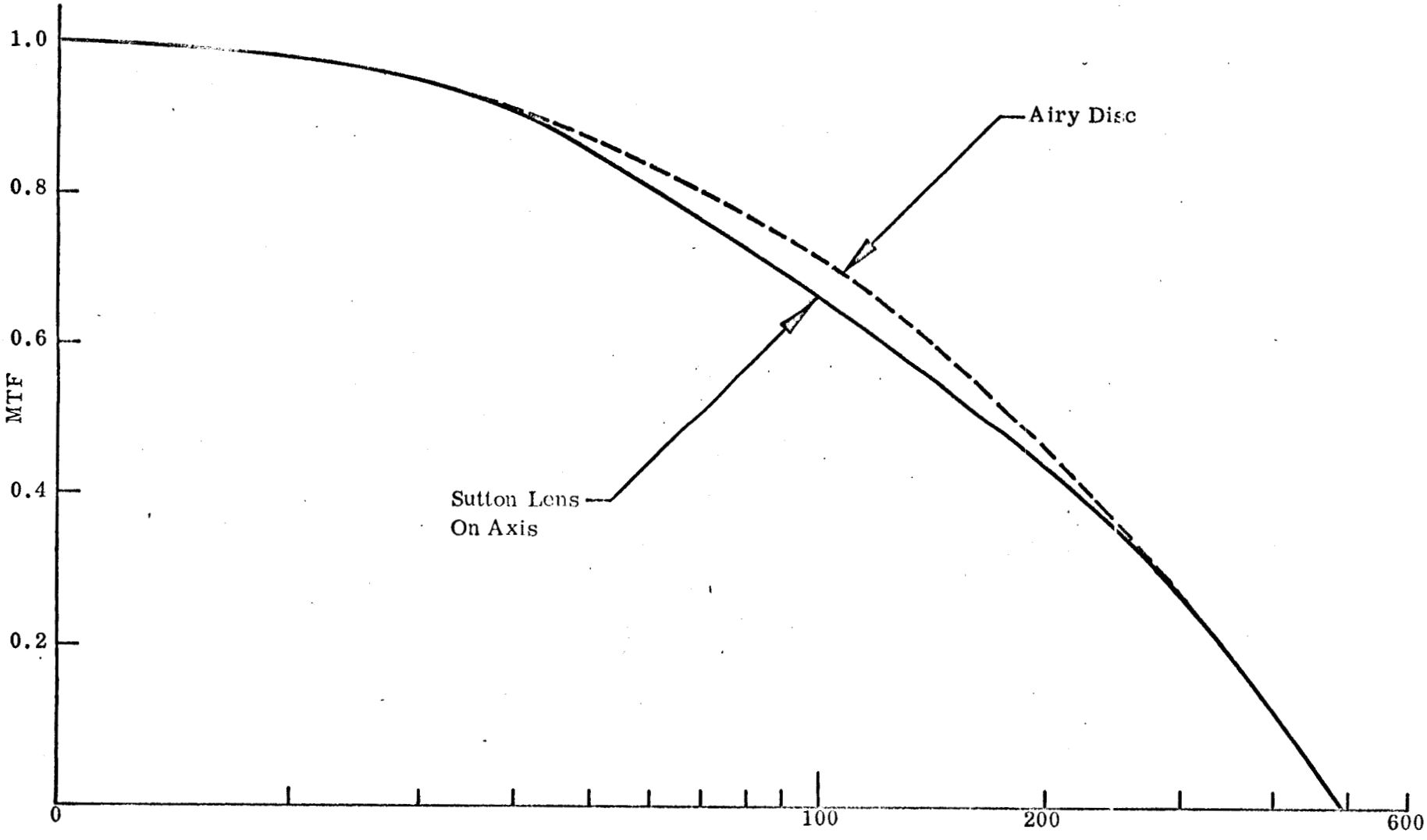

Figure 29 - MTF of Sutton Lens

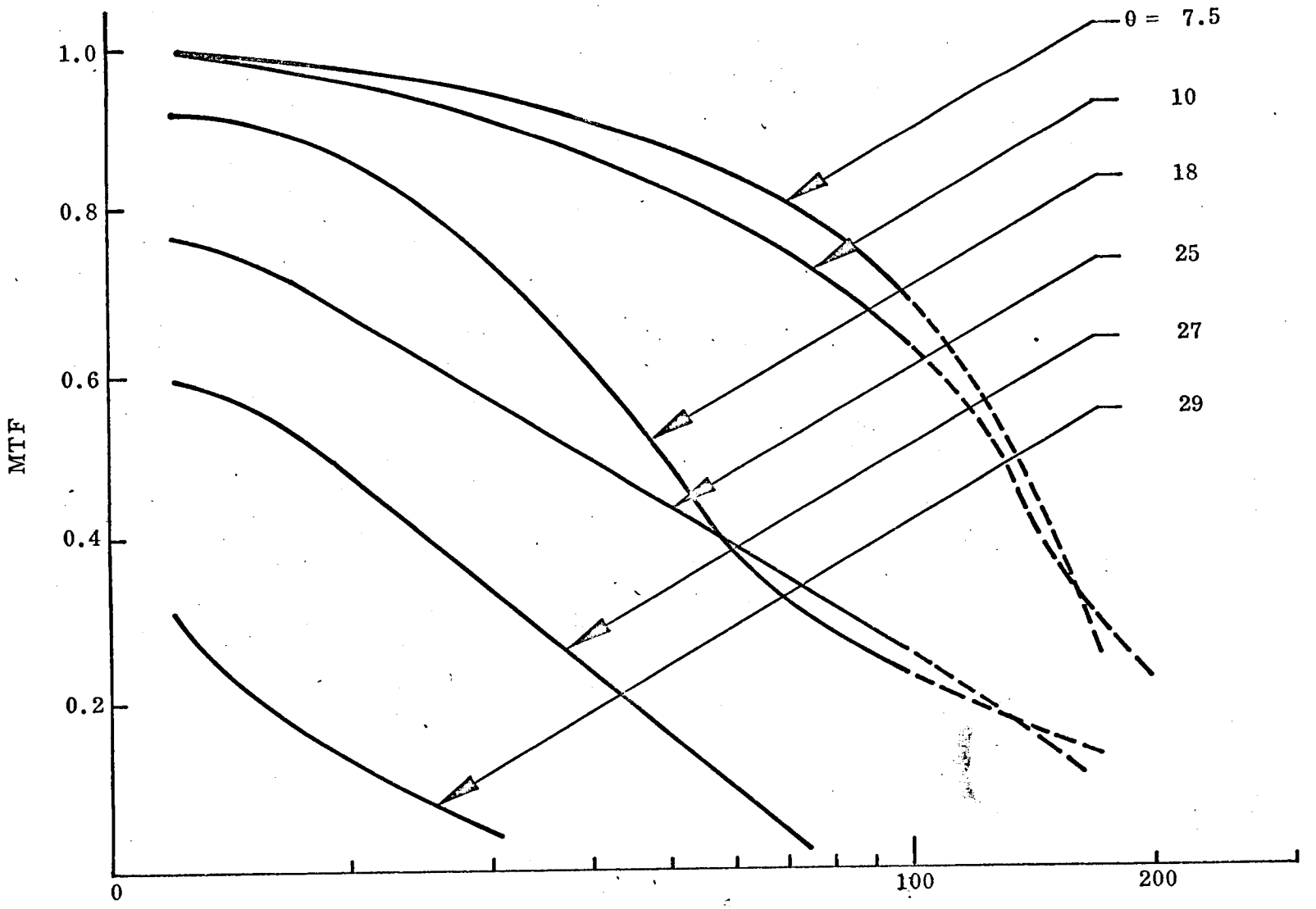

Figure 30 - MTF of Field Flattener Fabricated from 0.97 N.A., EMA-Coated Fibers

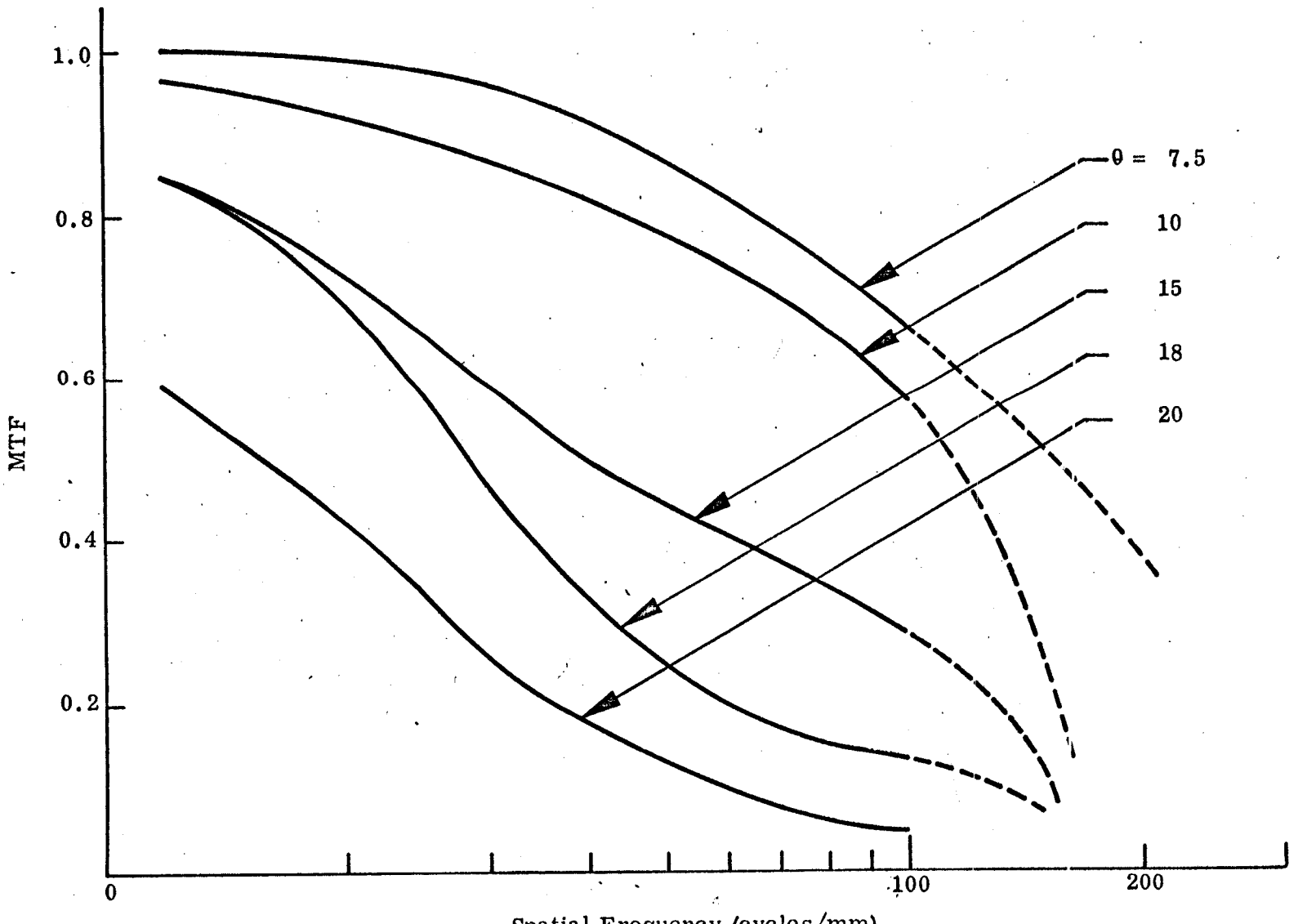

Figure 31 - MTF of Field Flattener Fabricated from 0.73 N.A., EMA-Coated Fibers

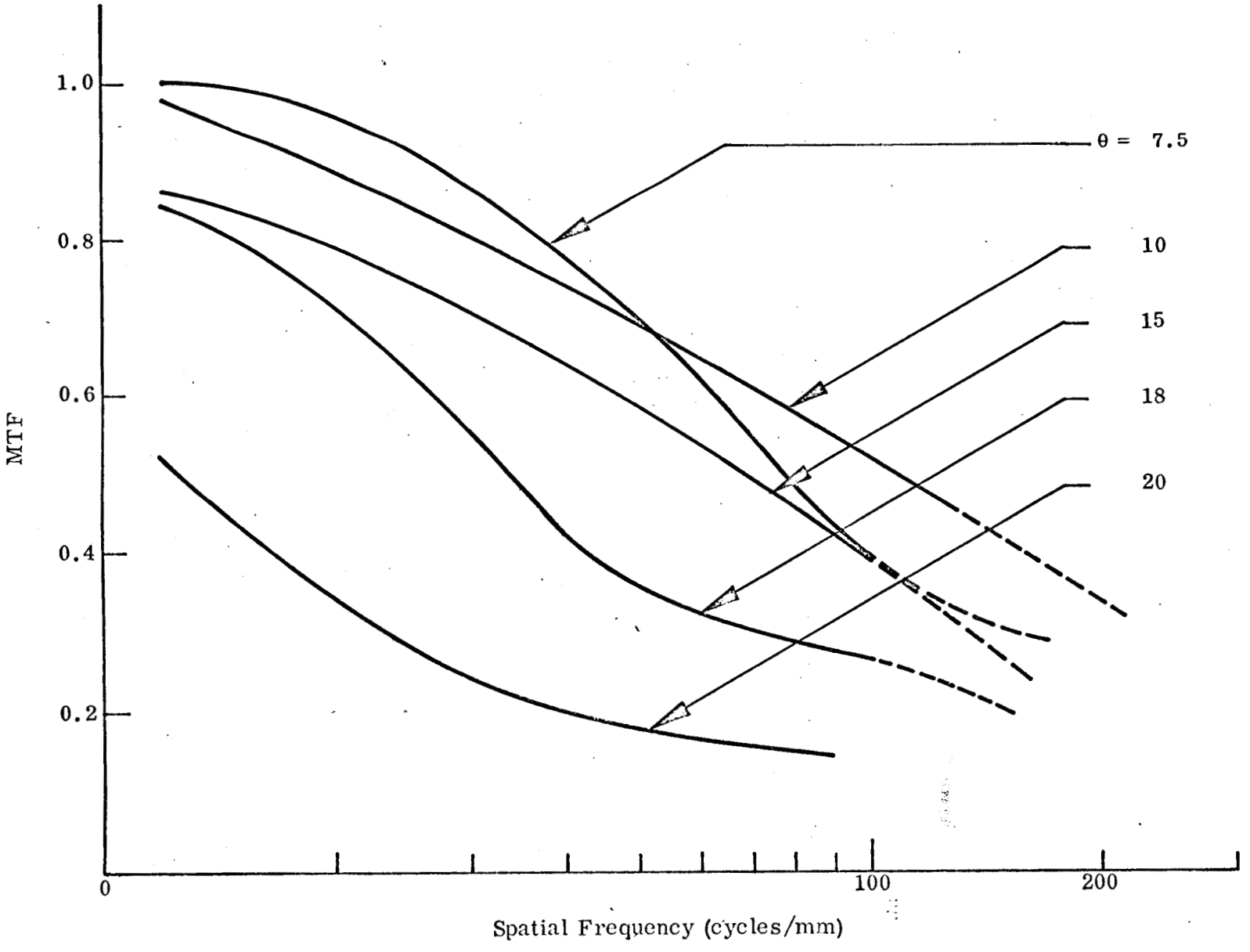

Figure 32 - MTF of Field Flattener Fabricated from 0.73 N.A. Fibers, without EMA Coating

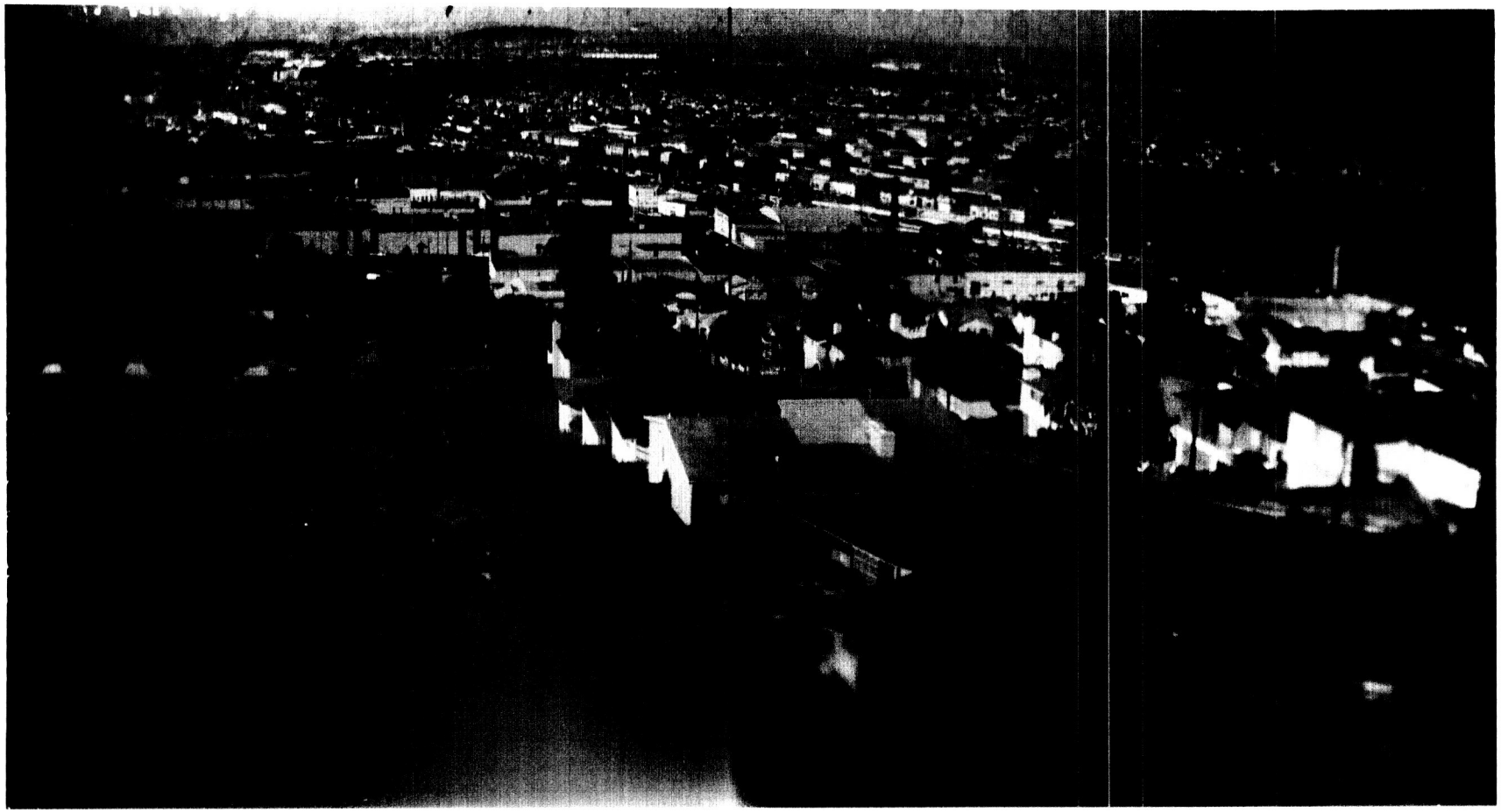

Figure 33 - Photograph Taken Through the Sutton Lens Camera with Field Flattener

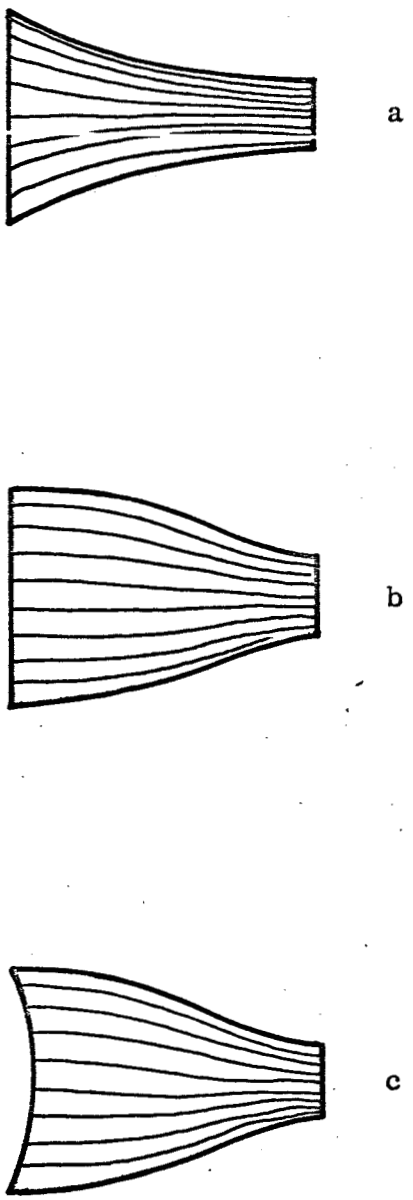

Figure 34 - Typical Focon Configurations

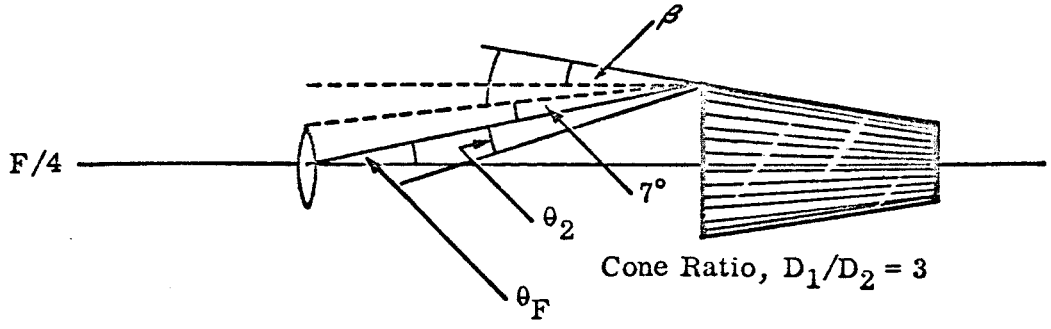

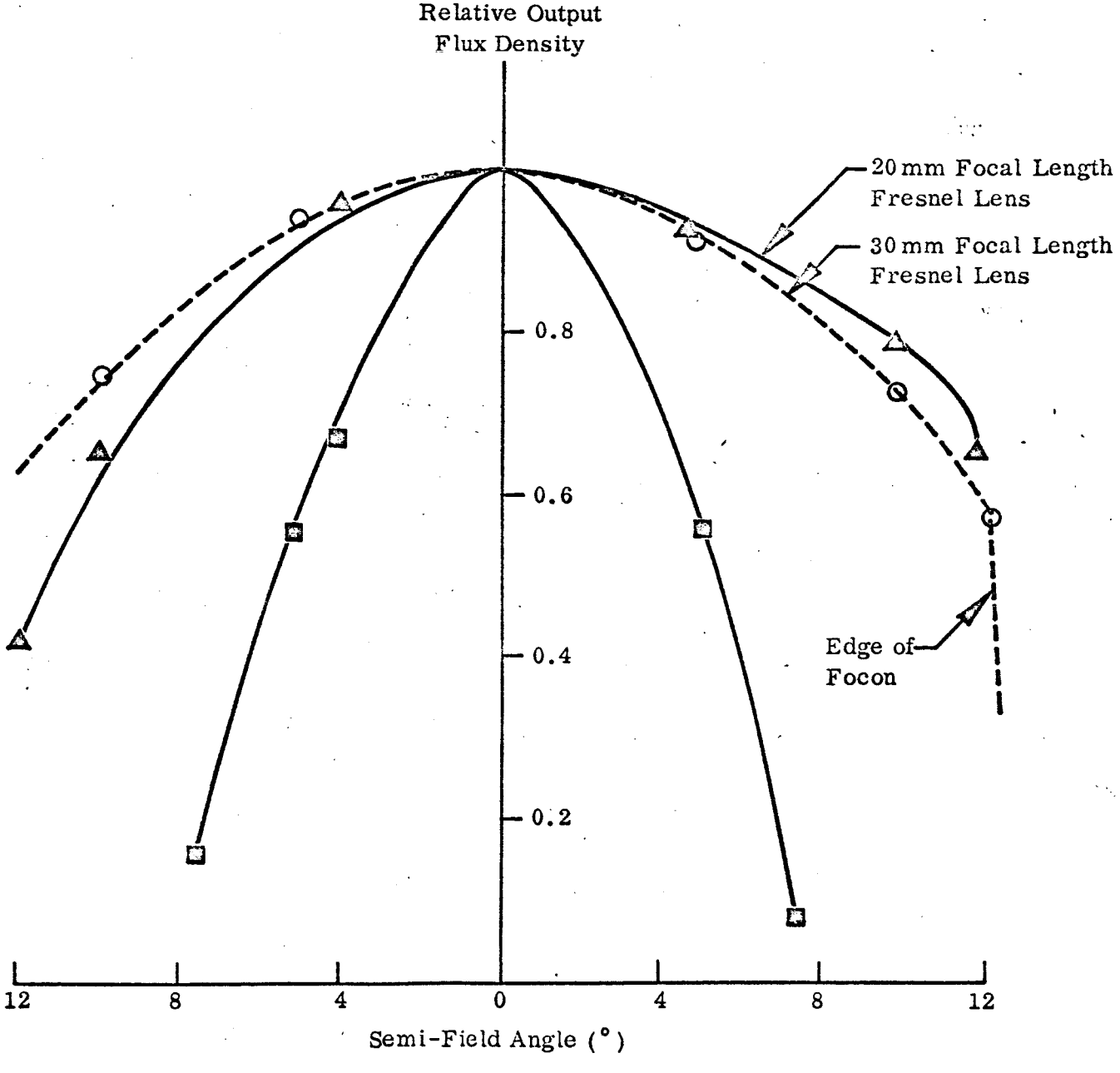

Figure 35 - Vignetting of a Focon

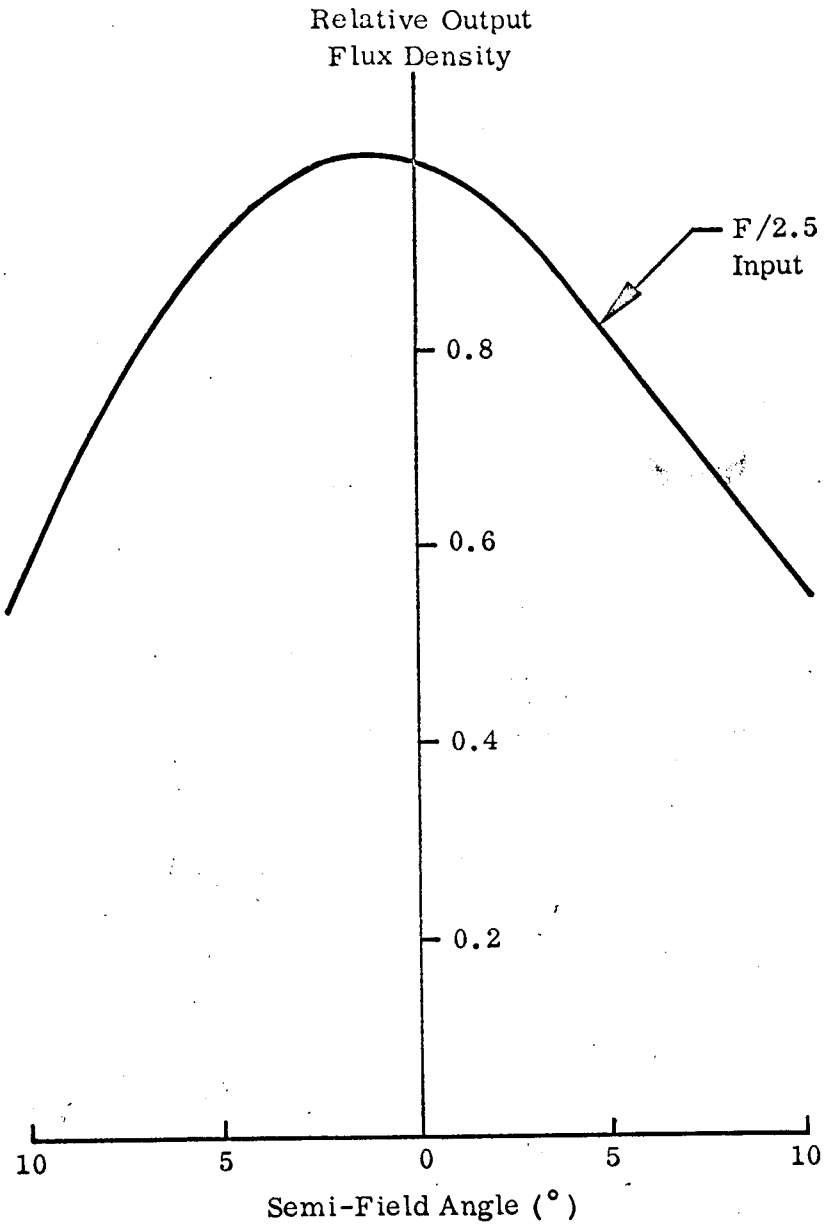

Cone No. 14b

Cone ratio at center of field	= 2.5
Cone ratio at edge of field	= 2.7
Theoretical speed gain at edge of field	= 6.2
Actual speed gain at center	= 3.2
Output F/No. on axis	= 1.4

Figure 36 - Vignetting of a Focon

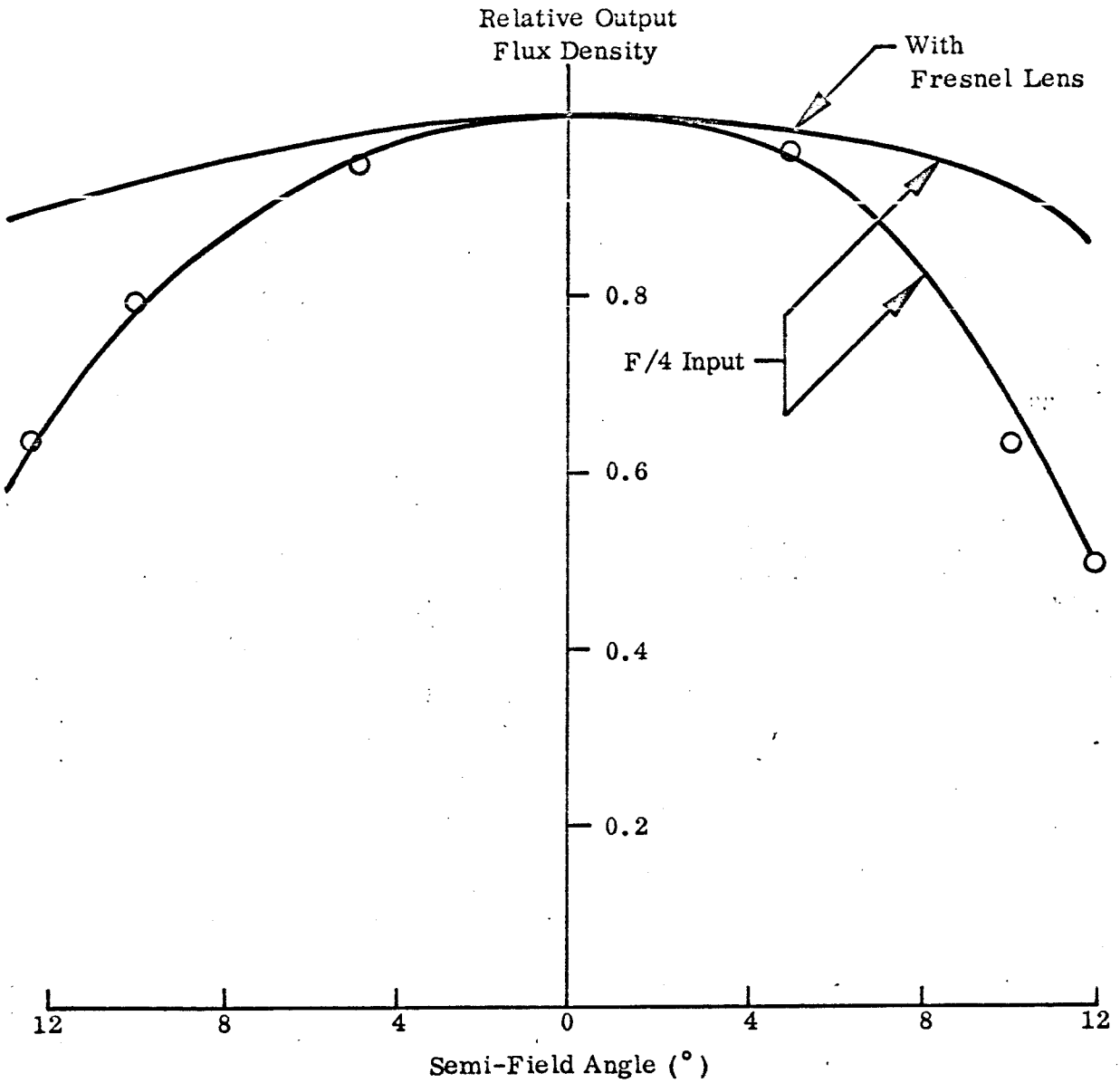

Cone No. 18/1

Cone ratio = 2.7
Theoretical speed gain = 7.3
Actual speed gain = 2.4
With an F/4 input beam

Figure 37 - Vignetting of a Focon

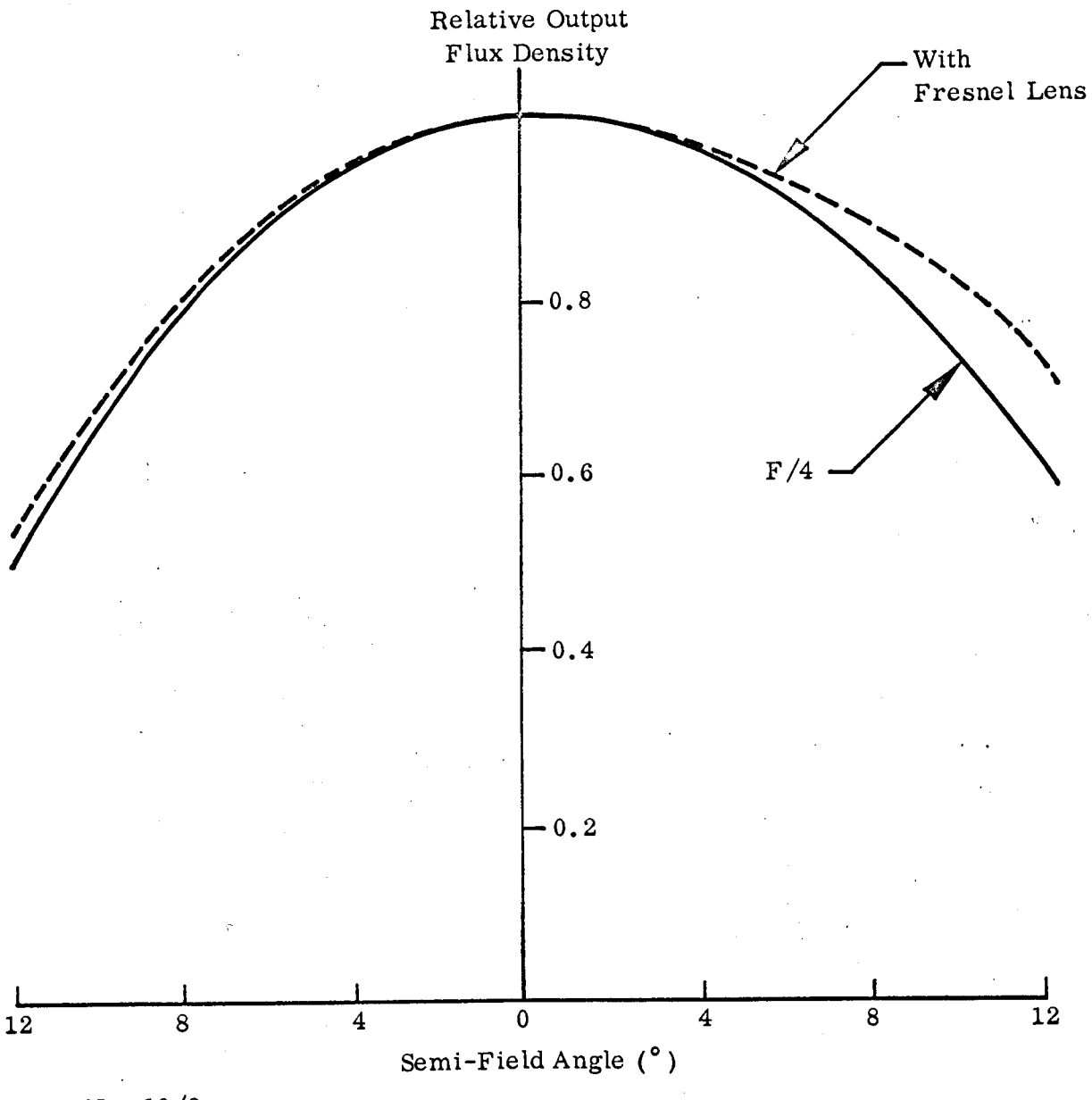

Cone No. 18/2

Figure 38 - Vignetting of a Focon

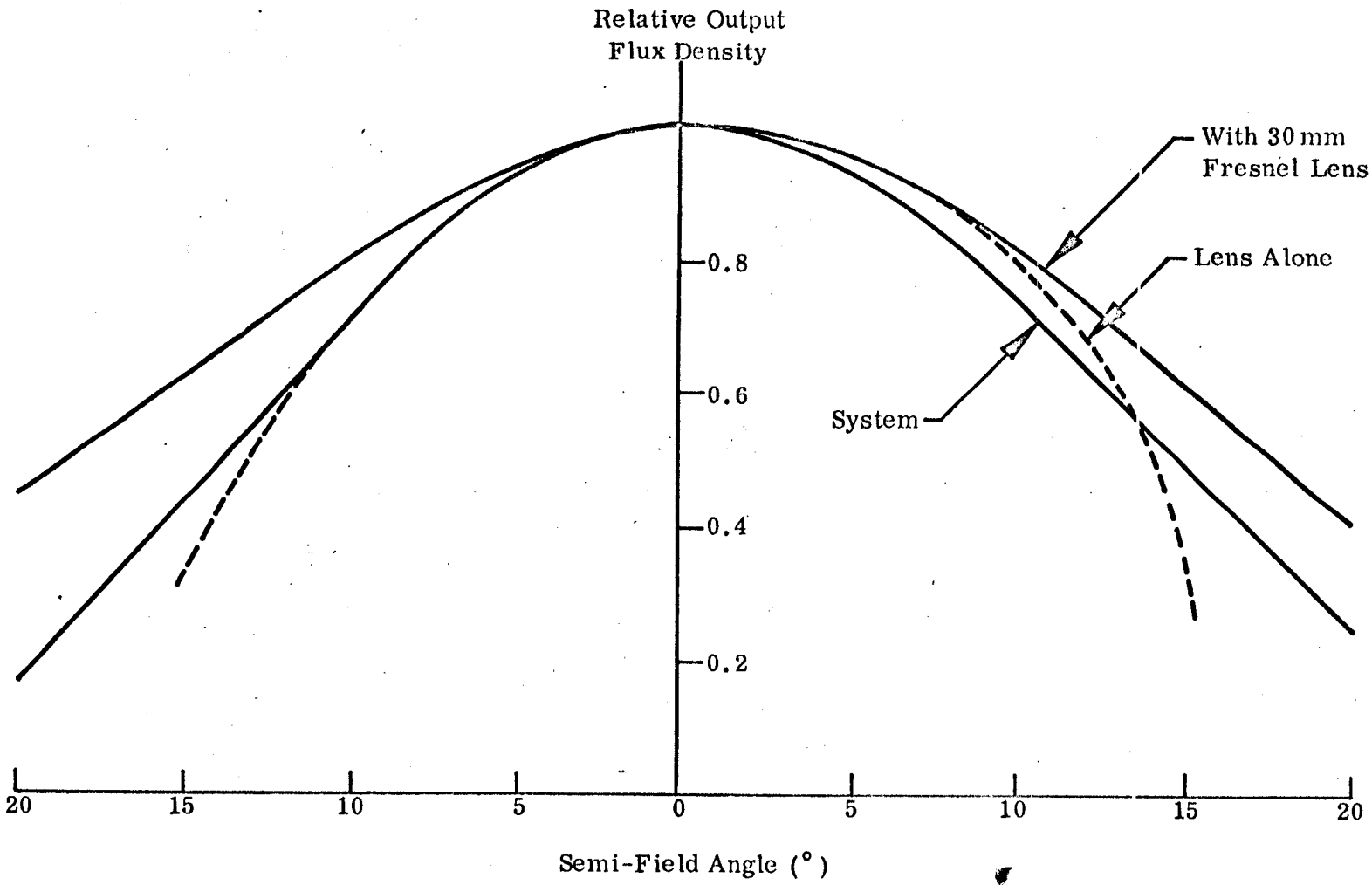

System Vignetting with an F/2.3,
30 mm focal length objective lens

Cone ratio = 2.9
Speed gain = 3.1
Equivalent output F/No. = 1.32

Figure 39 - Vignetting of a Focon

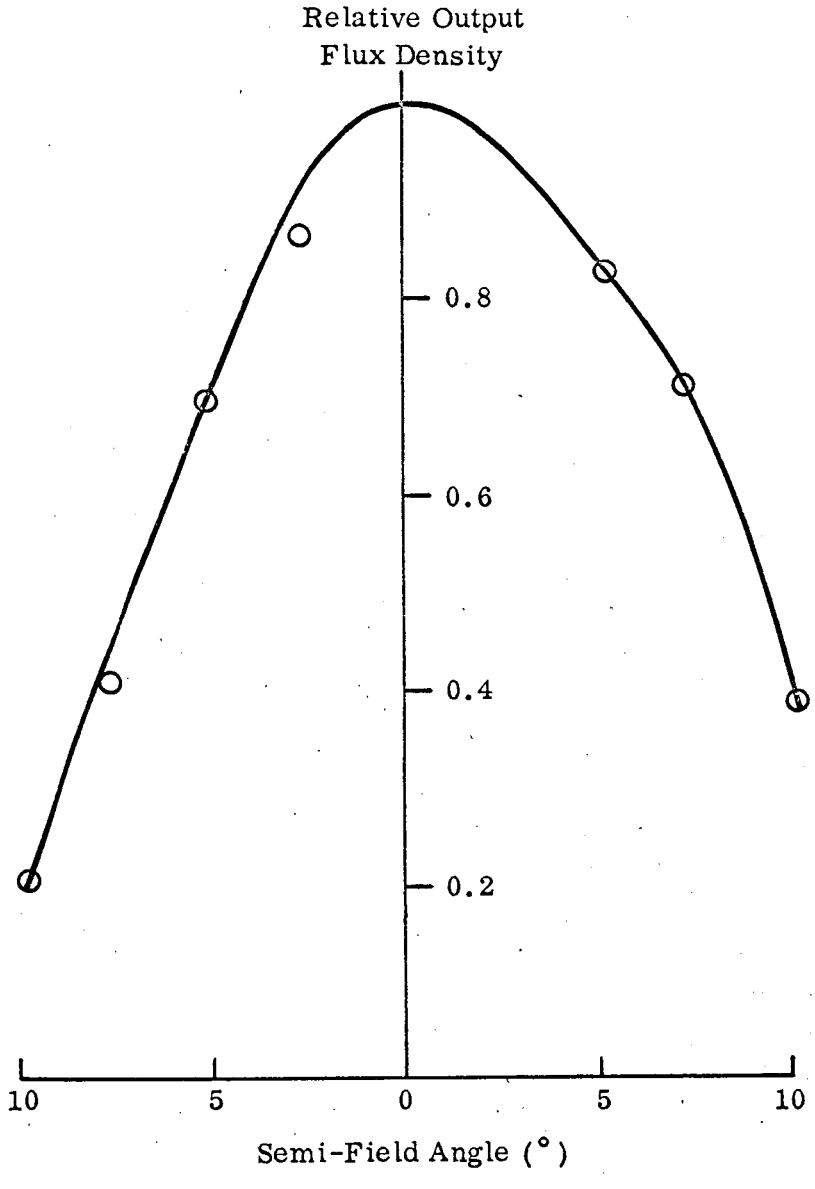

Cone 14a

2 in. Radius, Spherical
Input Surface

Figure 40 - Vignetting of a Focon and Field Flattener

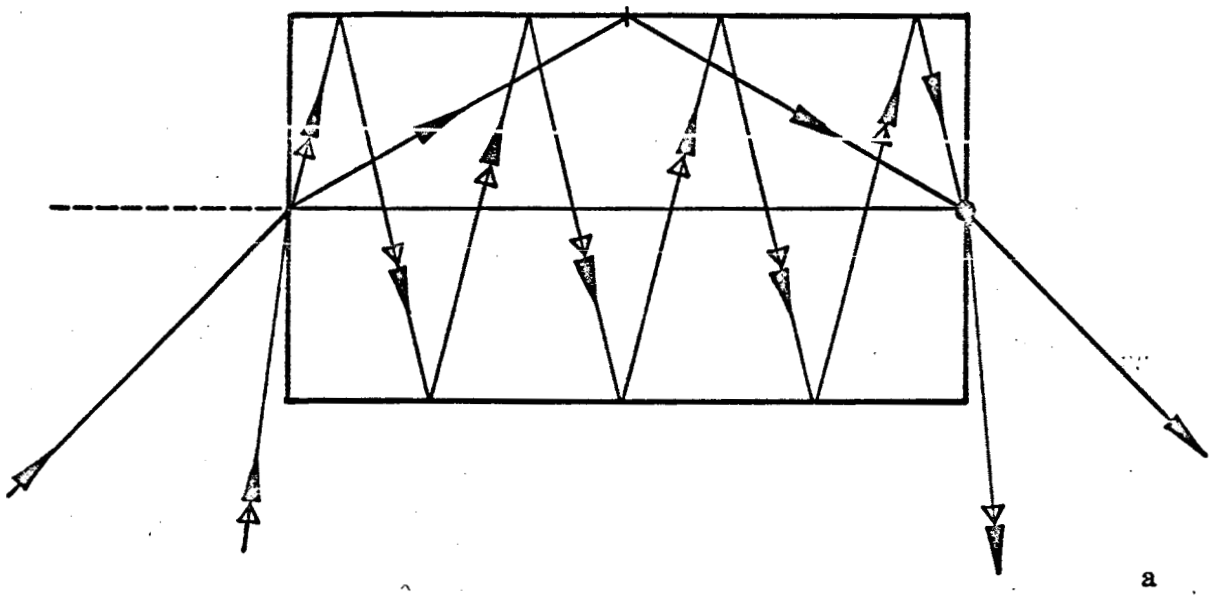

a

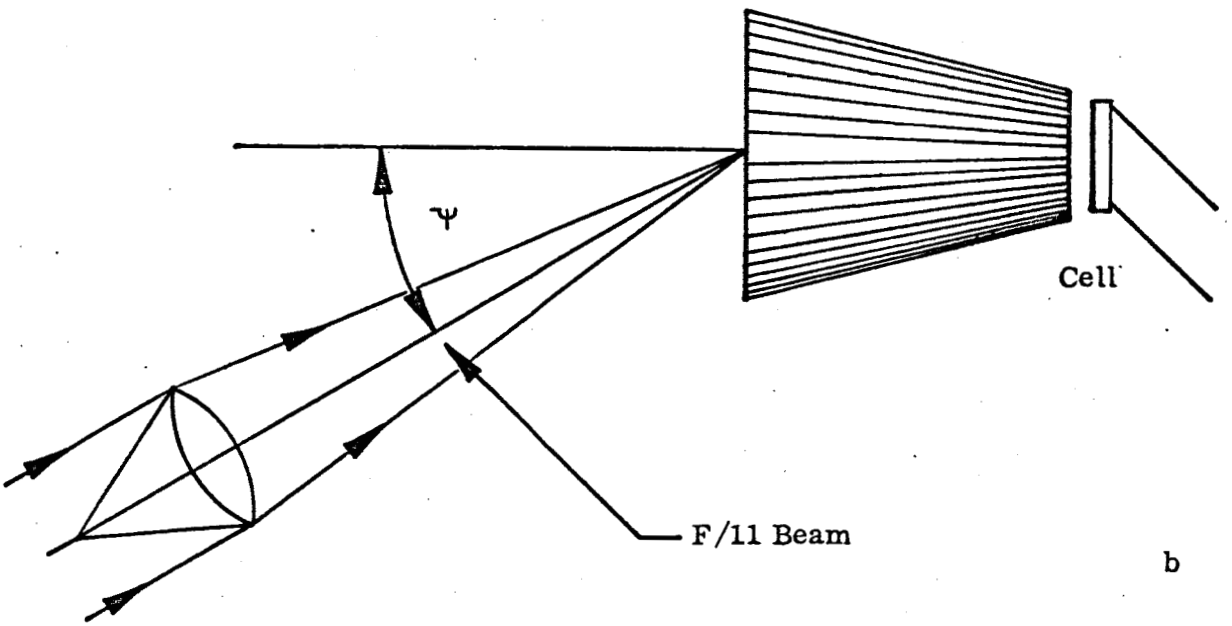

b

Figure 41 - Schematic of Apparatus for Determining the Variation in the Fresnel Reflection Losses at the Focon Output as a Function of Angle of Incidence

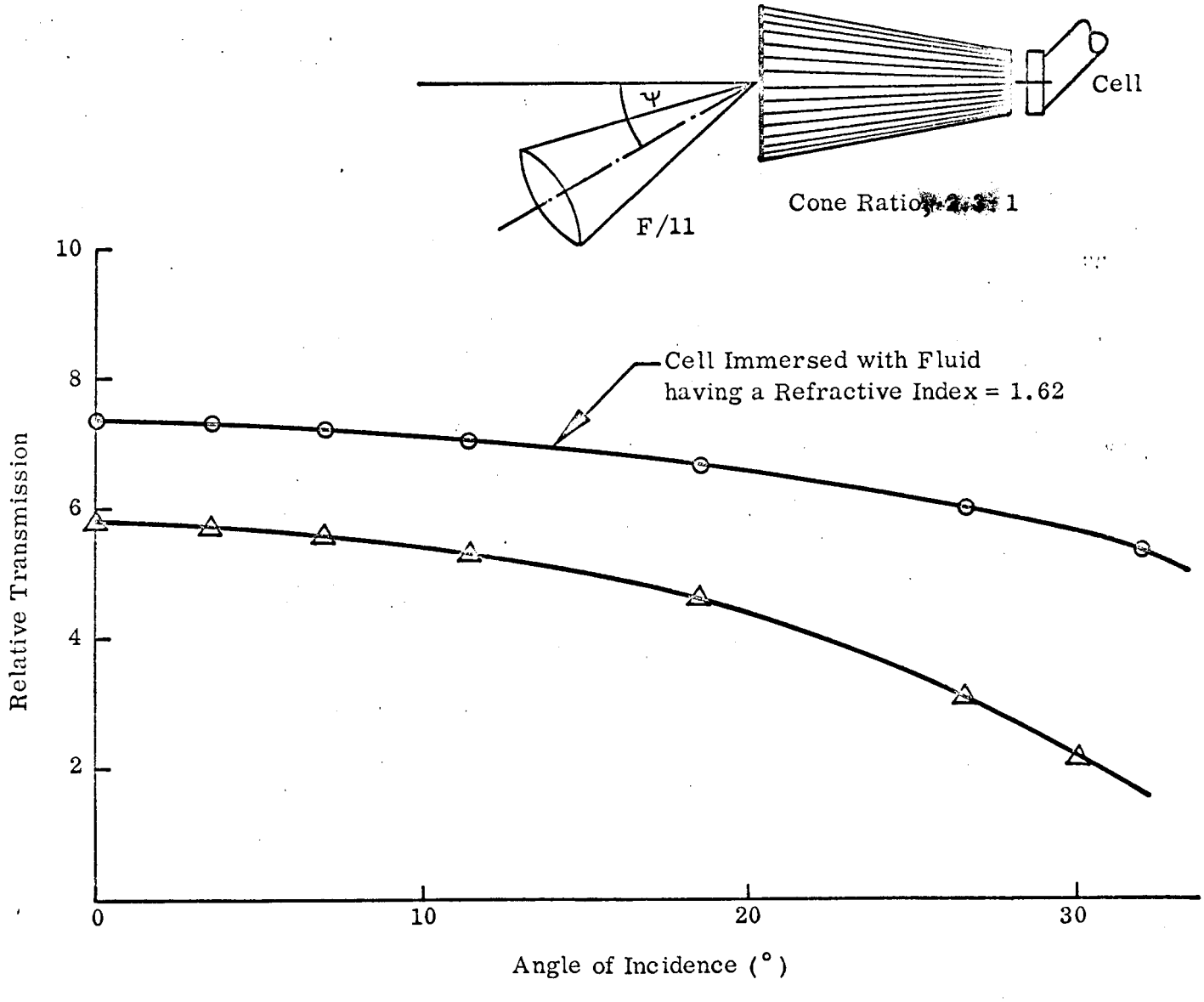

Figure 42 - Comparison of Focon Vignetting as a Function of Angle of Incidence with the Focon Output Both Coupled and Uncoupled to the Detector

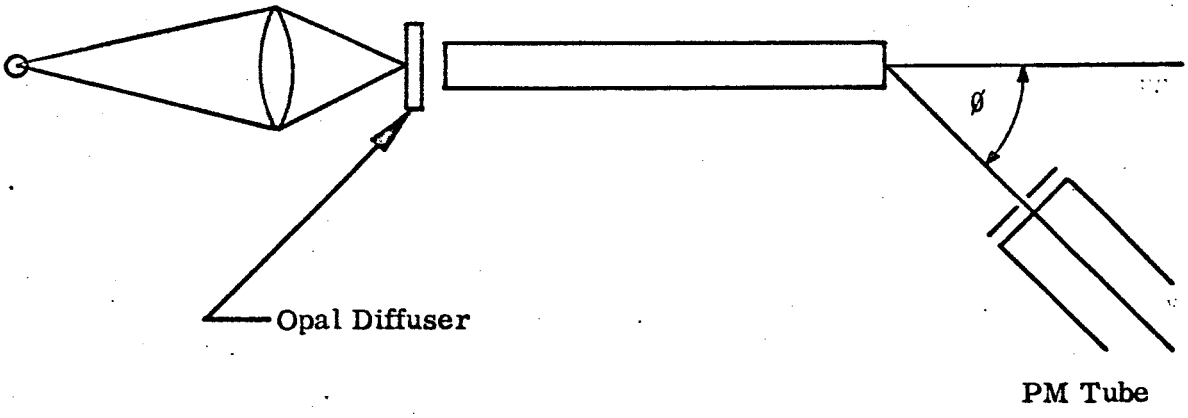

Figure 43 - Schematic of Apparatus for Determining the Radiation Patterns of Single and Multiple Fibers

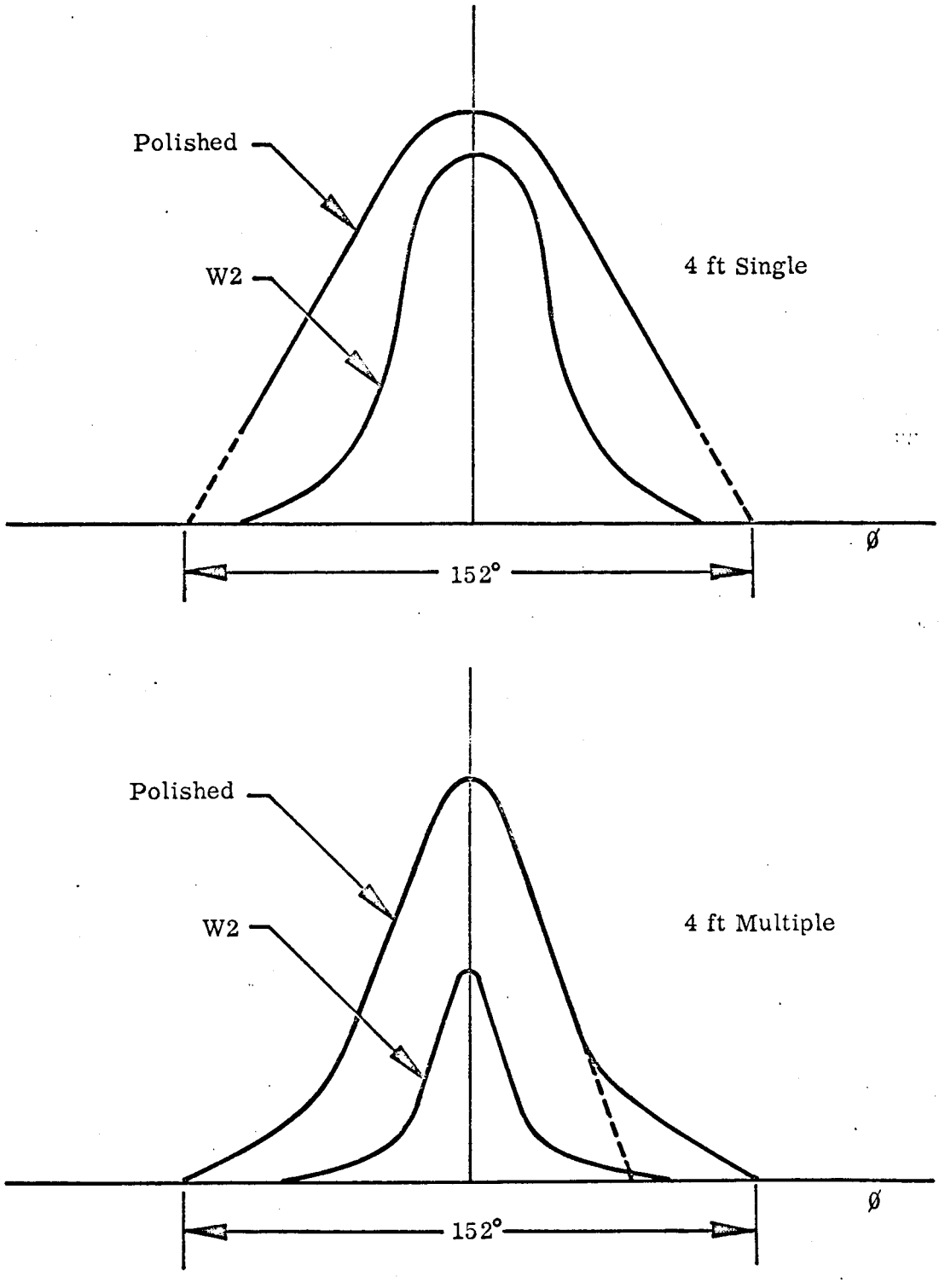

Figure 44 - Radiation Patterns of Single and Multiple Fibers

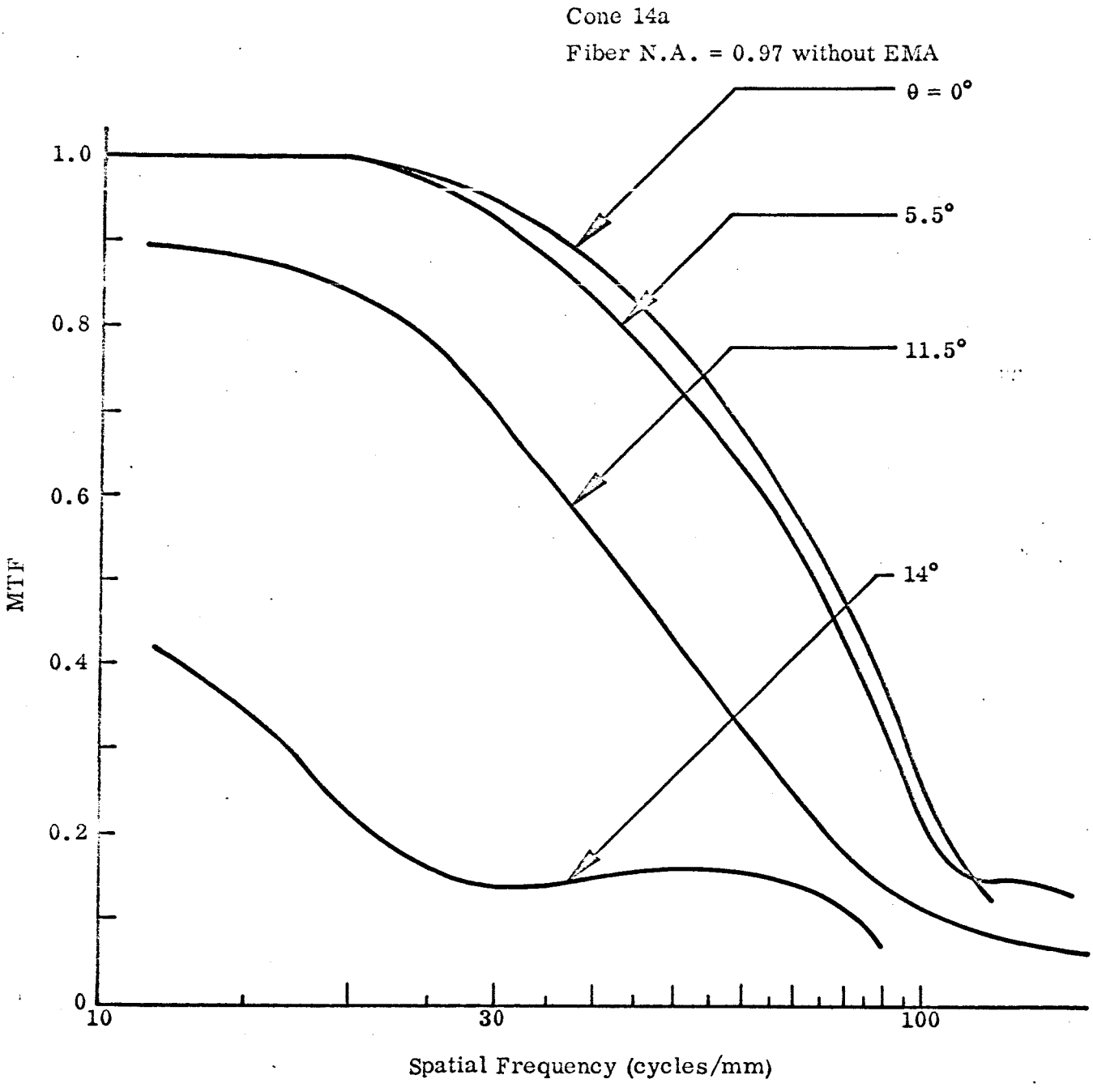

Figure 45 - MTF for Various Field Angles θ of a Sutton Lens + a Focon with a Field Flattener at the Input Face of the Cone

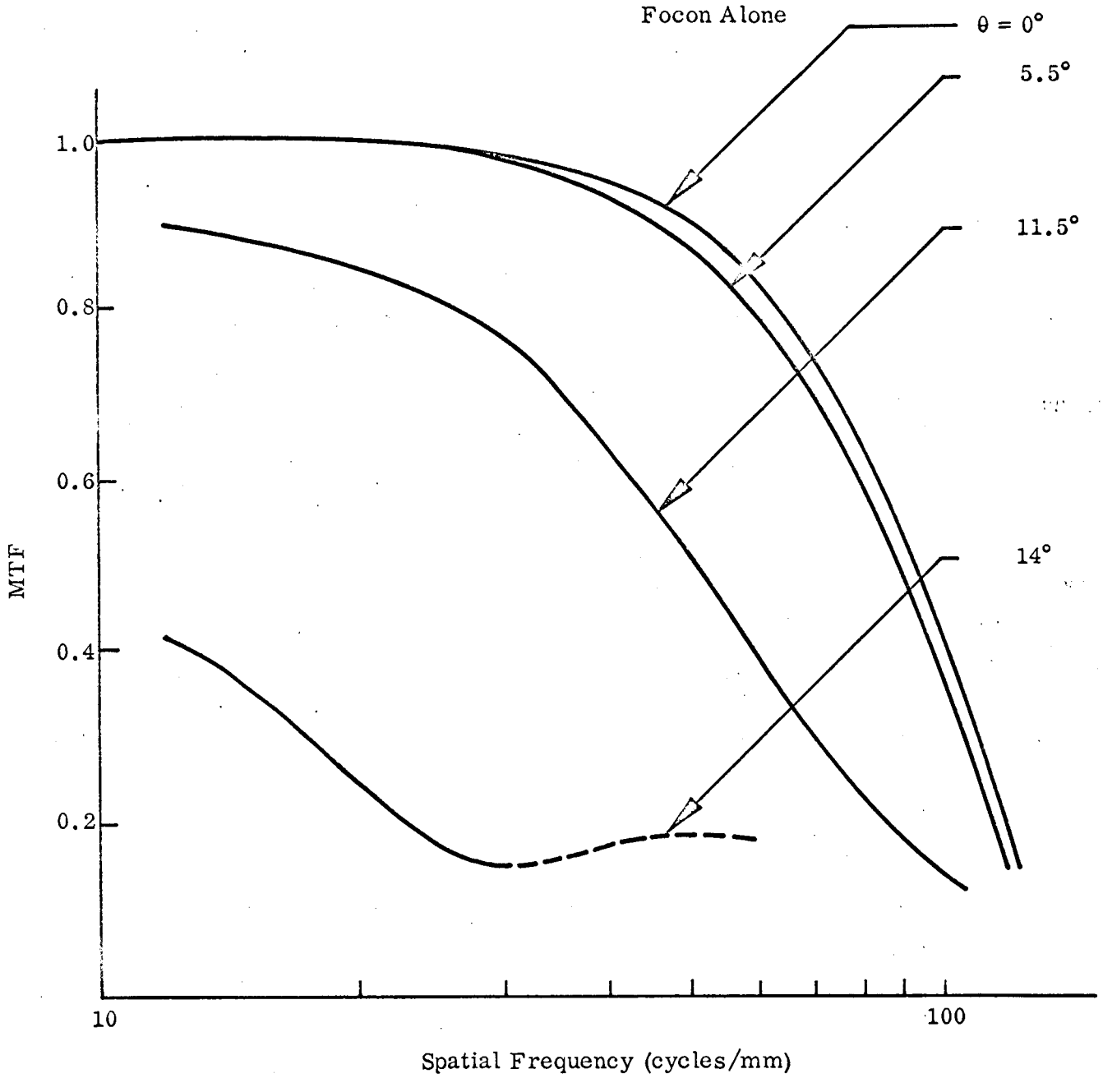

Figure 46 - MTF for Various Field Angles θ of a Focon with a 2-inch Radius Field Flattener Input Face